MIT Thesis Template in Overleaf

by

Tim Beaver

Submitted to the Department of Electrical Engineering and Computer Science
in partial fulfillment of the requirements for the degree of

Bachelor of Science in Computer Science and Engineering

at the

MASSACHUSETTS INSTITUTE OF TECHNOLOGY

June 1990

Author .....
Department of Electrical Engineering and Computer Science
May 18, 1990

Certified by .....
William J. Supervisor
Associate Professor
Thesis Supervisor

Accepted by .....
Arthur C. Chairman
Chairman, Department Committee on Graduate Theses

MIT Thesis Template in Overleaf

by

Tim Beaver

Submitted to the Department of Electrical Engineering and Computer Science
on May 18, 1990, in partial fulfillment of the
requirements for the degree of
Bachelor of Science in Computer Science and Engineering

Abstract

Lorem ipsum dolor sit amet, consectetur adipiscing elit. Nam quis neque et erat laoreet finibus at ac leo. Curabitur pellentesque, diam quis dignissim finibus, enim dui feugiat leo, nec porttitor sapien mi ac felis. Nam aliquam pretium nibh, quis dapibus dolor gravida sit amet. Cras porttitor dui quis elementum pulvinar. Nulla id pulvinar massa. Nullam ut diam non lorem venenatis faucibus. Vivamus lacus ante, pellentesque vitae nisl sit amet, bibendum facilisis purus.

Thesis Supervisor: William J. Supervisor
Title: Associate Professor

Acknowledgments

This is the acknowledgements section. You should replace this with your own acknowledgements.

Contents

List of Figures

List of Tables

Chapter 1

Introduction

In this thesis, I will provide a complete treatment of occluder-based imaging. The thesis is split into two main sections. The first section will be focus on the question of designing *optimal* occluders. The natural application of this kind of research is generally within context of designer mask-based cameras. The second section will be about methods for exploiting *accidental cameras*, which means using occlusion provided by objects that happen to be in the world to image hidden scenes.

Although there is obviously a close relationship between these two areas of research, and I will use a common framework for analyzing both they are nevertheless distinct, and which one the reader is interested in will depend on the application they are interested in.

I will begin my thesis by describing in detail the analytic framework that I use for both, and introducing the assumptions I use and the optical model that underlies them. My hope is that even without much or any background in optics, all my readers will have no trouble understanding the model and assumptions I use, and my mathematically-savvy readers will have no trouble understanding the conclusions that follow from them.

I highly recommend that *any* reader begins by reading the chapter that follows before proceeding to either of the two main sections (on optimal occluders and on accidental cameras). Without this background, I expect that it will be difficult to understand what I'm saying.

Chapter 2

The Model and Assumptions

2.1 Ray Optics and BRDFs

Throughout my thesis, unless I say otherwise, I'll be using the *ray optics model* of light. This means that, as a convenient abstraction, I'll be assuming that light moves in a straight line through the air, can be bent when it hits a different light-propagating medium (like a lens), and may be absorbed or reflected by the materials it hits (like a wall). Moreover, I'll be generally assuming that light intensity is additive, meaning that two rays of light hitting the same point will generate an intensity equal to the intensity that would be generated the sum of each individual ray. This corresponds to assuming that the light we care about is incoherent and as such won't interfere with itself—a reasonable assumption when the light in question is coming from the sun or from a commercial electric light. Finally, using the ray optics model means that I'll be ignoring the effects of diffraction, which is reasonable when modeling the behavior of visible-wavelength incoherent light hitting macroscopic structures. If this paragraph was hard to understand, don't worry—just take it to mean that light travels in straight lines, bounces off stuff it hits, and generally does what you intuitively think it should.

What happens when the light hits an opaque surface, according to this model? Some of it will be absorbed, and some reflected. How much of it is reflected, and in what directions, is described by the *bidirectional reflectance distribution function*, or

BRDF, of the surface. The BRDF is a function from *incident*, or incoming, angle of the light to the outgoing angle of the light. It's best explained with two example BRDFs, which happen to describe the many of the surfaces we care about.

The first example BRDF is called the *specular* BRDF, and surfaces that have this BRDF are called specular surfaces. The typical example of a specular surface is a mirror. The specular BRDF takes the incident light and flips it across the surface normal. How can we describe this mathematically? We can describe it using a function of two arguments, the first being the angle of the incident light, θ_{in} and the second being the angle of the outgoing light, θ_{out}. Each angle is given from the surface normal. [1]Here, the specular BRDF we want is:

$$f_{\text{specular}}(\theta_{\text{in}}, \theta_{\text{out}}) = \begin{cases} \rho & \text{if} \theta_{\text{in}} = \pi - \theta_{\text{out}} \\ 0 & \text{otherwise} \end{cases}$$

The ρ here is a constant that determines the overall brightness of the surface in question—how much of the light is actually reflected rather than absorbed or transmitted. For example, for a mirror, ρ might be almost 1, meaning that almost all the light is reflected, but for a window where most of the light is transmitted rather than reflected, ρ might be much smaller, like 0.01 or 0.001.

The second example BRDF is called the *Lambertian* BRDF, after the 18th-century physicist Johann Heinrich Lambert. Surfaces that have this BRDF are often called *Lambertian*, *matte*, or *diffuse* surfaces, and I will use these terms interchangeably in this thesis. Intuitively, this BRDF takes the incoming light and scatters it "equally in all directions." Formally, here is the BRDF in question:

$$f_{\text{Lambertian}}(\theta_{\text{in}}, \theta_{\text{out}}) = \rho \cos(\theta_{\text{out}})$$

[1]If you're already familiar with the concept of BRDFs, you might be confused by this, since BRDFs are often described as functions of four real values. This confusion comes from the fact that for a 2D surface that lives in three dimensions, the angle of a light-ray from that surface is given by a 2D angle, which requires two real numbers to describe (one for the azimuth angle and one for the zenith angle). This is a detail that becomes unimportant if you treat each of the two arguments I'm describing as 2D angles, with equality between 2D angles achieved when both their azimuth angle and their zenith angle match. Here, to keep things simple, I'm implicitly assuming a 1D surface that lives in a 2D world, so angles are described by a single real number.

Once again ρ is a constant that determines the overall surface brightess. Note that the Lambertian BRDF is completely independent of the angle of the incident light—it scatters the light it reflects in exactly the same way no matter where the light came from.[2]

Now at this point, a careful reader may object: why did I claim that Lambertian surfaces scatter light "equally in all directions," when in reality, they scatter light in directions proportionally to that direction's cosine? Indeed, this is a major source of confusion when it comes to Lambertian surfaces. Google "Lambertian surface" or "Lambertian BRDF" and you will find about half your results defining it as I do, and half of them defining it instead as a perfectly constant function, depending neither on θ_{in} nor θ_{out}. This is an important confusion to resolve; I hope now to convince you beyond a doubt that my definition is the right one, and that the alternate definition of a Lambertian surface, while the objects it describes might exist in principle, in practice I've never seen one—whereas the objects my definition describes are all over the place. The walls and ceiling of the room you're sitting in, the paper you may be reading these words on, the clothes you're reading: all of these are nearly perfectly described by the Lambertian BRDF as I have defined it.

Here's where the confusion comes from. Find a sheet of paper. Lay it flat against a desk, then look at it from a few different angles. No matter what angle you look at it from, it looks equally bright.

At first, this seems it argues for the alternate definition of a Lambertian surface. After all, if you see the same amount of light coming from the sheet of paper no matter what direction you observe it from, doesn't that it mean that the amount of light it transmits is equal in all directions—that is, it doesn't depend on θ_{out}? In fact, no. Consider: depending on what angle you are looking at the sheet of paper from, the paper will take up a larger or smaller part of your field of vision. Look at the paper head-on, and it takes up a relatively large part of your field of vision; look at the paper from a very glancing angle, however, and it takes up just a sliver. And yet,

[2]For a 2D surface living in a 3D world, the Lambertian surface BRDF is exactly the same, but the cosine is of the outgoing zenith angle, and the outgoing azimuth angle doesn't matter.

no matter what the angle you observe it from is, you can still see the entire sheet of paper.

What's the upshot of this? What this means is that when you are looking at the sheet of paper from a very glancing angle, you are actually getting less total light from the paper, since the amount of light per amount-of-your-field-of-vision (sometimes called a "steradian") remains fixed, but the amount of your field of vision filled by the paper has decreased. And in fact, it has decreased by a factor of $\cos(\theta)$, where θ is your angle from the paper's normal. This is where the factor of $\cos(\theta)$ in the definition of the Lambertian BRDF comes from. Indeed, if the Lambertian BRDF sent light truly equally in all directions, as you looked at the paper from an increasingly glancing angle, the paper would appear to get *brighter*, in order to keep the total amount of light you were receiving from the paper constant. Some objects behave the opposite way, like backlit LCD screens; if you tilt them away from you, their apparent brightness will usually decrease (depending on the screen), which means that their BRDF is attenuated *faster* than $\cos(\theta_{\text{out}})$. But no object I've ever seen has a BRDF that is attenuated *slower* than $\cos(\theta_{\text{out}})$.

Most real-world surfaces lie on a spectrum somewhere between Lambertian and specular. This isn't to say that most real-world BRDFs are a linear combination of the Lambertian and specular BRDFs; an example of an object that *does* behave that way is a dirty or smudged mirror. But most objects aren't like that; they may look "shiny" or "glossy," but they don't give you a sharp-but-faint reflection, like a dirty mirror might. Rather, many glossy objects have BRDFs that send some light in all directions, but more light in directions where the outgoing angle be relatively close to the incident angle reflected across the surface normal. These BRDFs are often modeled using the "Phong" model, after the model described by Bui Tuong Phong in his PhD thesis. According to the Phong model, the extra light in the reflected directions (also called the "specular highlights") fall off polynomially with the the dot product of the outgoing angle with the reflected incident angle. The degree of that polynomial depends on the how shiny or dull the surfaces, with higher-degree polynomials yielding a smaller and more focused specular highlight.

In this thesis, the main focus will be on Lambertian surfaces. When I do consider the possibility of specular of Phong surfaces, I'll go into more detail about what exactly the BRDF model I'm using is at that time. So for the time being, let's consider what can happen using the simplest model that nevertheless describes much of reality very well: a 2D world of Lambertian surfaces.

2.2 The Far-Field Assumption

2.2.1 A point light source and a nearby surface

Let's suppose we live in a 2D world of Lambertian surfaces and diffuse light sources. (When I say a "diffuse" light source, I mean that the light source scatters light equally in all directions. Confusingly, this isn't quite the same thing as a "diffuse" surface—which is another way of saying a Lambertian surface, which actually doesn't quite scatter light equally in all directions, as I explained in the previous section—but that's how these terms are used.) Consider a point light source suspended at $(0, y_p)$, with a Lambertian surface at $y = 0$ (see Figure 2-1). What pattern of illumination can we expect to see on the surface?

The way we proceed with this analysis is to discretize the surface into many small chunks, and then to consider what fraction of the light radiating out of the point light source is hitting any single given small chunk of the surface. We assume each chunk is small enough that its luminance is constant across the chunk. Asking what fraction of light radiating out of the point light source hitting any given chunk is equivalent to asking what angle over the light source is subtended by that chunk, and then dividing that angle by 2π.

Supposing that the chunk extends from $(x_c, 0)$ to $(x_c + dx, 0)$, trigonometry tells us that θ_c, the angle subtended by the chunk, is given by:

$$\theta_c = \tan^{-1}\left(\frac{x_c + dx}{y_p}\right) - \tan^{-1}\left(\frac{x_c}{y_p}\right)$$

What happens as we consider increasingly smaller and smaller chunks dx? The def-

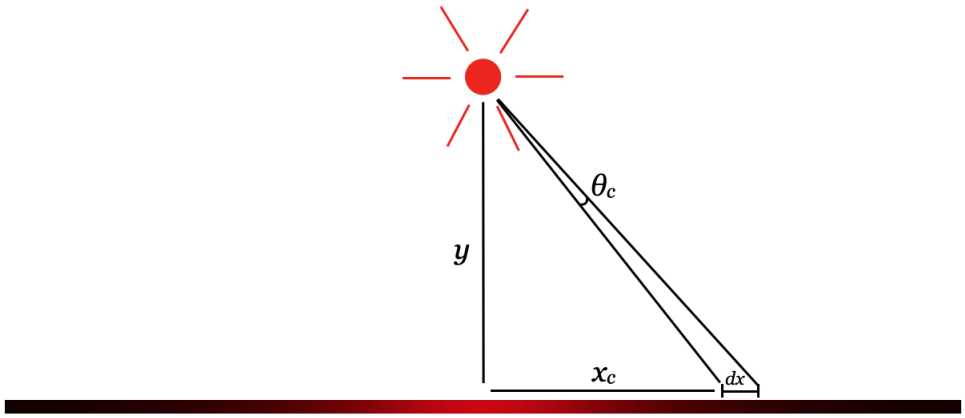

Figure 2-1: A diagram illustrating the following setup: a point light source at $(0, y_p)$, with a Lambertian surface at $y = 0$. We are interested in the resulting illumination pattern on the Lambertian surface; to investigate it, we measure the illumination of a small chunk on the surface that extends from $(x_c, 0)$ to $(x_c + dx, 0)$. The illumination of that chunk will be proportional to the angle θ_c of the point source's light subtended by the chunk.

inition of the derivative tells us that $\lim_{dx\to 0} \theta_c = dx \cdot \frac{d}{dx_c}(\tan^{-1}(\frac{x_c+dx}{y_p})) = dx(y_p/(x^2 + y_p^2))$. Thus the luminance of a chunk on the surface, assuming that the point source had a luminance of 1, would be $dx(y_p/(2\pi(x^2+y_p^2)))$.[3]We can say that the continuous illumination function of the surface $I(x)$ is the following:

$$I(x) = \frac{y_p}{2\pi(x^2 + y_p^2)}$$

This simple formula captures a lot of interesting phenomena. Consider for instance that we take $x = 0$, meaning we consider the illumination only of the closest point on the surface to the point source. The formula tells us then that the illumination of that point goes as $1/y_p$, meaning that it scales inversely with that point's distance from the point source. Now consider fixing $y_p = 1$ and varying x. This gives us a illumination pattern that scales with $1/(1 + x^2)$, a nice "hump" pattern. The closer the surface is to the point source (meaning a smaller y), the narrower the hump will be. (See Fig. 2-2) Also note that no matter what y_p is, we have:

[3]Readers who are unfamiliar with terms like "luminance" may be confused by a subtle distinction between what I mean by "luminance" versus "illumination pattern" or "brightness." When I talk about the "luminance" of something, I'm referring to the absolute amount of light that thing emits.

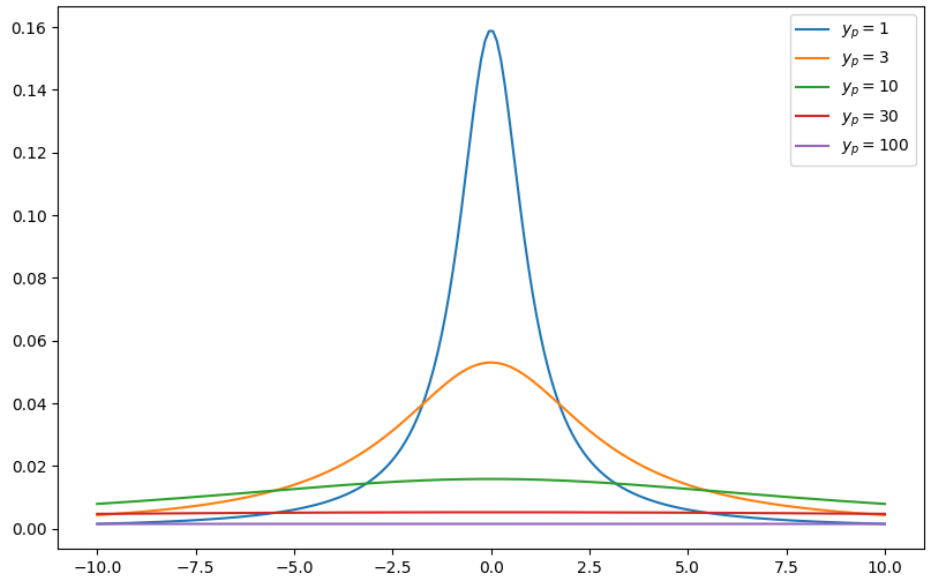

Figure 2-2: Different illumination patterns depending on different possible values of y_p, with the Lambertian surface extending from $x = -10$ to $x = 10$. As this plot shows, the far-field assumption starts to become reasonable for $y_p = 30$.

$$\int_{-\infty}^{\infty} \frac{y_p}{2\pi(x^2 + y_p^2)} dx = 1/2$$

It stands to reason that this is true, because no matter how far the surface is from the point source, if the surface is infinitely broad, exactly half the light from the point source will hit the surface. Additionally, for reference, I'll provide here the illumination function for the equivalent situation in three dimensions: a point source of luminance 1 suspended at $(0, 0, z_p)$, and a plane at $z = 0$. Then, the illumination function $I(x, y)$ can be derived in much the same way as in the two-dimensional case. This function is given by:

$$I(x, y) = \frac{z_p}{4\pi(x^2 + y^2 + z_p^2)^{3/2}}$$

In any case, the important thing to note at this point is that, as shown in Figure 2-2, the illumination pattern becomes flatter and broader the further the point source is from the surface. This phemonenon is what we rely on when we make the "far-field assumption." The far-field assumption is that the assumption that the contribution of a point light source to a faraway surface is approximately constant across that surface. As you can see, this assumption holds as long as the size of the surface in question is much smaller than the distance of the point source to the surface; that is, if, for all relevant values of x, $x^2 \ll y_p^2$, then it follows that $I(x)$ holds a constant value of approximately $1/(2\pi y_p)$ ($1/(4\pi z_p^2)$ in three dimensions), assuming the point source has a luminance of 1.

Because of the quadratic dependence on x and y_p in Eq. **??**, the far-field assumption yields a reasonable approximation even when the difference between x and y_p isn't enormous; for example, if you hold a diffuse light source three meters away from the center of a flat surface two meters in diameter, the brightness of that surface

In contrast, when I use the term "brightness" or "illumination pattern," I'm referring to the light emission *density* of that thing. When you look at a surface, that surface's apparent brightness is proportional to how much light it emits per area of your vision it occupies. So whereas the *luminance* of a small surface chunk in the example given above would be $dx(y/(2\pi(x^2 + y^2)))$, to get the *brightness* of that same surface chunk we'd want to divide by its area; hence its brightness would be $y/(2\pi(x^2 + y^2))$. This makes sense: the apparent brightness of a surface shouldn't depend on how finely you choose to discretize it!

won't vary by more than about 16% (compare $1/9^{3/2}$ to $1/10^{3/2}$). The far-field assumption gets relied on very heavily, both in my research and in work by others, and admittedly the reason for that isn't that it's always a hugely robust assumption to real-world situations (after all, depending on the application, sometimes 16% can matter a lot!). The reason, rather, is that it's an extremely *convenient* assumption. For the time being I'll leave it at that, but in later sections we will see that tolerating the far-field assumption allows us to solve quite a few different optics problems in closed form, or reduce them to easy rather than difficult problems of linear algebra. When I can I will extend my analysis to cases where the far-field assumption cannot be made.

2.3 The Standard Setup

In this section, I will briefly describe what I call "the standard setup," and introduce some terminology that I will use throughout the dissertation. The simplest version of the standard setup is shown in Fig **??**: three parallel frames in flatland, with the "intermediate frame" halfway in between the scene and the observation plane. The presumption is that the observation is a known quantity, and we'd like to infer what's in the scene. Depending on the details of the problem, the intermediate frame may also be a known quantity, or its form may be unknown. In any case, we'd like to see how much we're able to infer about the scene from the observation thanks to (or despite!) the presence of the intermediate frame.

The term "intermediate frame" is left deliberately vague. In an ordinary camera, the intermediate frame would be a lens. In most of this dissertation, I'll be considering intermediate frames that don't directly focus the light from the scene like a lens would, but partially occlude the scene. In principle, there are any number of other realistic intermediate frames.

Of course, there are many other ways to relax the standard setup to make it richer or more realistic. The intermediate frame need not be halfway in between the observation plane; the three frames need not be parallel to each other; the scene

need not be planar. And, of course, the real world isn't flatland! But the standard setup is a great starting point for any optical analysis. Colloquially, the form that analysis might take is that an intermediate frame is better for imaging with if, given its presence, the observation tells us more about the scene.

2.3.1 The Transfer Matrix

Another critical concept in my dissertation is the *transfer matrix.* The transfer matrix is a matrix that describes the action of an intermediate frame on the scene to create the observation. To be more precise, suppose we approximate the scene by a vector $\vec{x}$, where each entry of that vector gives the illumination of a single chunk of the scene. Suppose that we approximate the observation plane in the same way with a vector $\vec{y}$. Then, the transfer matrix, A, will be whichever matrix satisfies $\vec{y} = A\vec{x}$ for all possible pairs $(\vec{x}, \vec{y})$.

How do we know that such a matrix even exists for all intermediate frames? Well, if we accept the assumptions implicit the ray-optics model described in Sec. 2.1—that is, we ignore the effects of diffraction and assume that light is incoherent—then what you observe should be a linear function of the presence or absence of light sources. That means that we call what you see if light a is on $f(a)$, and what you see if light b is on $f(b)$, then what you see when both lights are on, $f(a+b)$, should be the sum of what you saw in either case, $f(a) + f(b)$. You can try this at home! If you have a room which is perfectly dark when the lightswitch is off, see what the room looks like when you turn the lights are on versus when you turn on a lamp or flashlight. The brightness of every part of your room when both the lightswitch and lamp are on should roughly correspond to the sum of how bright there were when each were on individually.[4]The fact that this works in most real-world settings tells us that the assumptions of the ray-optics model aren't leading us too far astray.

[4]If you do this, what you see may not "feel" like it actually correspond to the sum of the two room brightnesses. For example, if you have two lights that both illuminate your room equally well, turning both on may not once may not feel like it's giving you a room that's "twice as bright." Make no mistake, though—that's not the fault of the ray optics model, that's the fault of your lying eyes! "Perceived brightness" is a bit of a slippery concept, but it isn't linear in the actual amount of light hitting your retina. In the same way that a 70 dB sound (vacuum cleaner) doesn't sound like it's

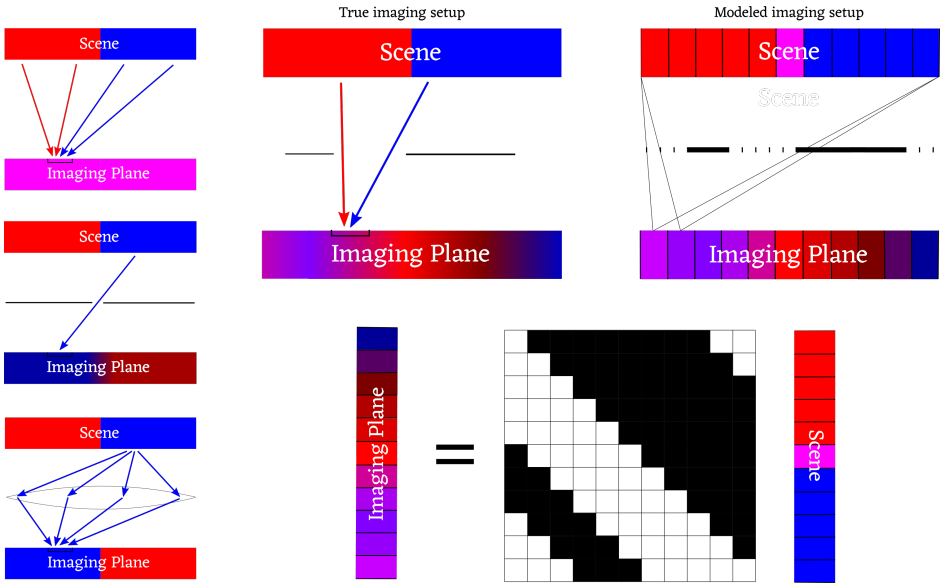

Figure 2-3: Three imaging systems (left, top-to-bottom): no aperture, a pinhole and a lens. Arrows indicate paths light from the scene takes to a particular point on the imaging plane. On the right is an arbitrary mask, an illustration of its discretization and the corresponding transfer matrix.

Because we're assuming that combining light sources behaves linearly, most real-world objects we can put in between a scene and an observation plane should be representable by a transfer matrix A. But what do matrices like these actually look like? Well, they can look like a variety of different things; Figure 2-3 shows the action of a variety of example intermediate frames, with an example transfer matrix corresponding to one of them.

So suppose we have a scene x, an observation y, and a transfer matrix A that represents how the intermediate frame distorts the scene to produce the observation. If $y = Ax$, and we know A and y, what transfer matrices A are best? In the absence of noise, any full-rank transfer matrix A should allow us in principle to perfectly reconstruct $x = A^{-1}y$. That makes the question of which transfer matrix not very interesting—it's a multi-way tie between all full-rank transfer matrices, which make up the vast majority of possible transfer matrices.

"half as loud" as an 80 dB sound (garbage disposal), 100 lumens doesn't look "half as bright" as 200 lumens.

2.3.2 Noise

Of course, it's unrealistic to expect no noise. Every real-world imaging setting will have at least some noise, and in any case it's the presence of noise that makes the problem interesting, and lets us distinguish between better and worse transfer matrices, even if both matrices have the same rank.

Adding noise, our new equation becomes:

$$y = Ax + \eta$$

where η is another vector representing random noise. Now that we have introduced a random variable into our equation, we will need to provide a probability distribution not only for η (to describe how the noise is distributed) but also for x.

Let's start by discussing the probability distribution of the scene vector, x. The simplest model to begin with is to have each entry of the scene be independent and identically distributed (IID), and drawn from a Gaussian. For example, suppose that each entry of the scene vector x was independently drawn from a Gaussian with a mean of μ and a standard deviation of σ. To describe this situation, we can write:

$$x \sim \mathcal{N}(\mu I, \sigma^2)$$

Before we can proceed with this model, there are a few problems for us to worry about. The first is possible negative entries. Real scenes don't cast negative light! To solve this problem, we take $\mu \gg \sigma$. That way, the probability of negative entries will be vanishingly small. A vanishingly small chance of a negative entry is good enough for us; it means that our model's distance from the real world due to this issue (where negative entries are impossible) is also vanishingly small.

The next problem is subtler: recall that x is a discrete vector, but it is meant to represent a continuous scene of fixed size. We haven't yet talked about the number of entries in x, which we'll call n. The variable n controls how finely we discretize the scene x. Ideally, choosing n to be larger will mean that our discrete representation of the true continuous scene will be more faithful (though perhaps at a computational

cost). And we might also hope that once n gets large enough, that's a close enough to the real scene that increasing it further won't make the model noticeably better. That's not such an unrealistic expectation; after all, if you're reading these words on a laptop screen, you're probably looking at a discrete array of a couple thousand by a thousand pixels, and that's plenty enough to give you the impression of a "continuous image" on your screen. Tripling the number of pixels on your laptop without increasing the size of your screen probably won't improve your impression of how "continuous" your screen looks by much, unless you're very good at noticing this kind of thing.

We'll talk more about exactly what we mean by this concept later (i.e, how finely we need to discretize the scene before we consider that to be "good enough"). For the time being, though, we have a more serious problem. The problem is this: varying n should give us representations of the true, continuous scene that are varyingly faithful. However, choosing a different value of n shouldn't qualitatively change what the scene looks like. It should always give us the closest discrete approximation possible to the true, continuous scene.

So first, we need to make sure that the total luminance of the scene (in other words, the total amount of light the scene emits) doesn't depend on n. But we said earlier that each entry of x was IID with a mean of μ, so at the moment the total luminance of the scene is $n\mu$. This means that μ is going to have to depend on n; in particular, we'll say that $\mu = J/n$, where J is a constant that represents the total luminance of the scene.

Our difficulties don't stop there, though. If each entry of x is IID and drawn from a Gaussian, then if we want the scene to be qualitatively the same independent of n, σ must also depend on n. In this case, what we mean by "qualitatively the same" is a little bit fuzzy, but we might make it formal by asking that scenes with $n = k$ be drawn from the same distribution as scenes with $n = 2k$ that are then "pixelated" by a factor of 2. (To "pixelate" a vector by a factor of k is to average groups of k contiguous pixels together—for example, if we pixelated the vector [1,2,3,4,5,6] by a factor of 2, we would be left with the vector [1.5, 3.5, 5.5].) By this definition, we

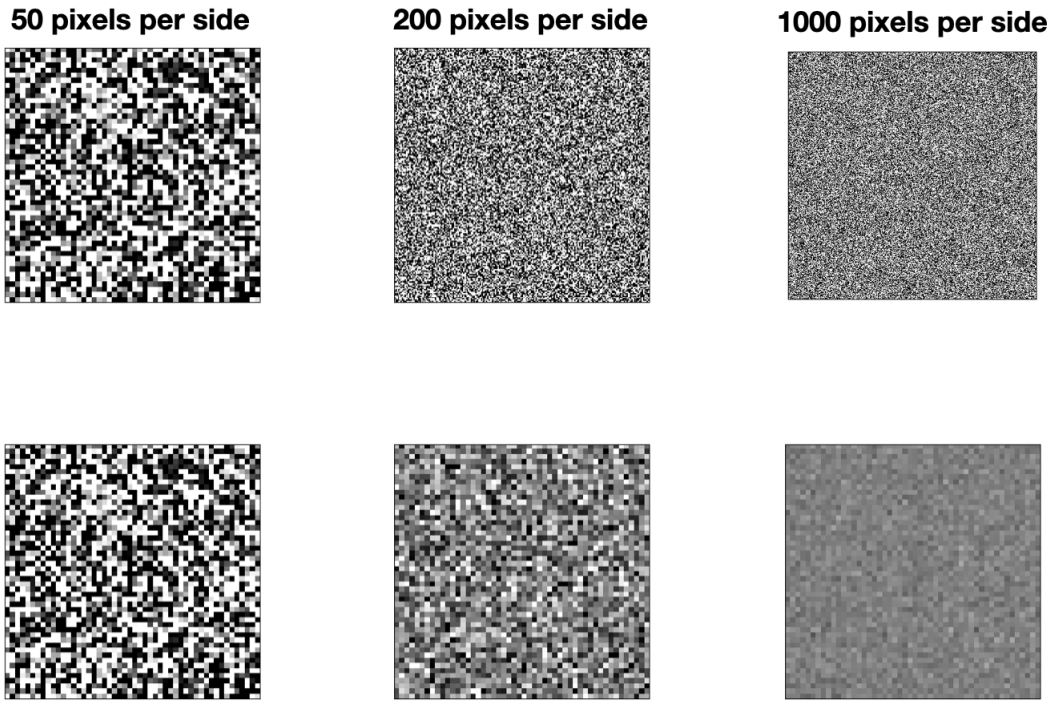

Figure 2-4: Top row: IID scenes with $\sigma = 1$, with three different levels of scene discretization ($n = 50$, $n = 200$, and $n = 1000$). Bottom row: each of those scenes, pixellated so that they have 50 pixels to a side. As you can see, the pixellated scenes look different from each other—this is a problem, because how finely we choose to discretize the scene shouldn't make a difference to what the scene looks like. This is why IID scenes of different levels of discretization are qualitatively different from each other, unlike correlated scenes whose covariance matrices are chosen carefully to scale properly with discretization level.

would need σ to actually *increase* linearly with n in order to have the finer-discretized scenes be less-pixelated versions of the coarser ones! And this is a problem because we said that $\mu \gg \sigma$, and that needs to be true for all values of n, which will be impossible if σ grows with n and μ shrinks with n. If this is hard to follow, see Figure 2-4 for an illustration of this issue.

So what's the solution? The solution is for our model of the scene to include correlations between nearby pixels. We can do this by supposing that the covariance matrix of the scene includes off-diagonal elements:

$$x \sim \mathcal{N}(Q, \sigma^2)$$

The covariance matrix Q captures the correlations between nearby pixels. In real scenes, the closer together two pixels are, the more correlated they'll become. Our model should be faithful to this as well—and in doing so, we will simultaneously create the situation we wanted before, in which scenes with different values of n look qualitatively similar to each other, just at different levels of fidelity.

To make things concrete, I'll provide an example of a scene covariance matrix, which I'll call the *exponential-decay prior*. Recall that an IID covariance matrix would just be a multiple of the identity, $Q = \frac{\theta}{n} I$, where θ is a constant in n. The exponential-decay prior is given by $\mathbf{Q} = \mathbf{F}_n^* \mathbf{D}^\star \mathbf{F}_n$, where $\mathbf{F}_n$ is the normalized DFT matrix of size n and $\mathbf{D}^\star$ is a diagonal matrix with the following entries: $d_1 = 1$, $d_i^\star = d_{n-i+1}^\star = \frac{\theta}{n} \beta^{\frac{i-1}{\lceil (n-1)/2 \rceil}}, i = 2, \ldots, \lceil (n+1)/2 \rceil$, for some frequency decay rate parameter $0 < \beta < 1$. A lower β implies a more strongly correlated scene.

It will be easier to make sense of all this if you look at Figure 2-5 to see for yourself what these covariance matrices look like, and what scenes generated from them look like.

2.3.3 Noise

Now that we have a model of the probability distribution over scenes, we need a model for the probability distribution over the noise. This crucially depends on what application it is we care about. We'll try and make the noise model general enough to apply well to all cases.

We distinguish between two different types of noise.

(Thermal noise): This includes noise sources that are independent of the contribution to the measurements due to the scene of interest. That means that the thing causing the noise isn't light coming from the scene; it's light coming from somewhere else (i.e. "glare"). We model it as additive Gaussian with variance W/n, where W denotes the constant net noise power and each pixel absorbs power proportional to its size, giving

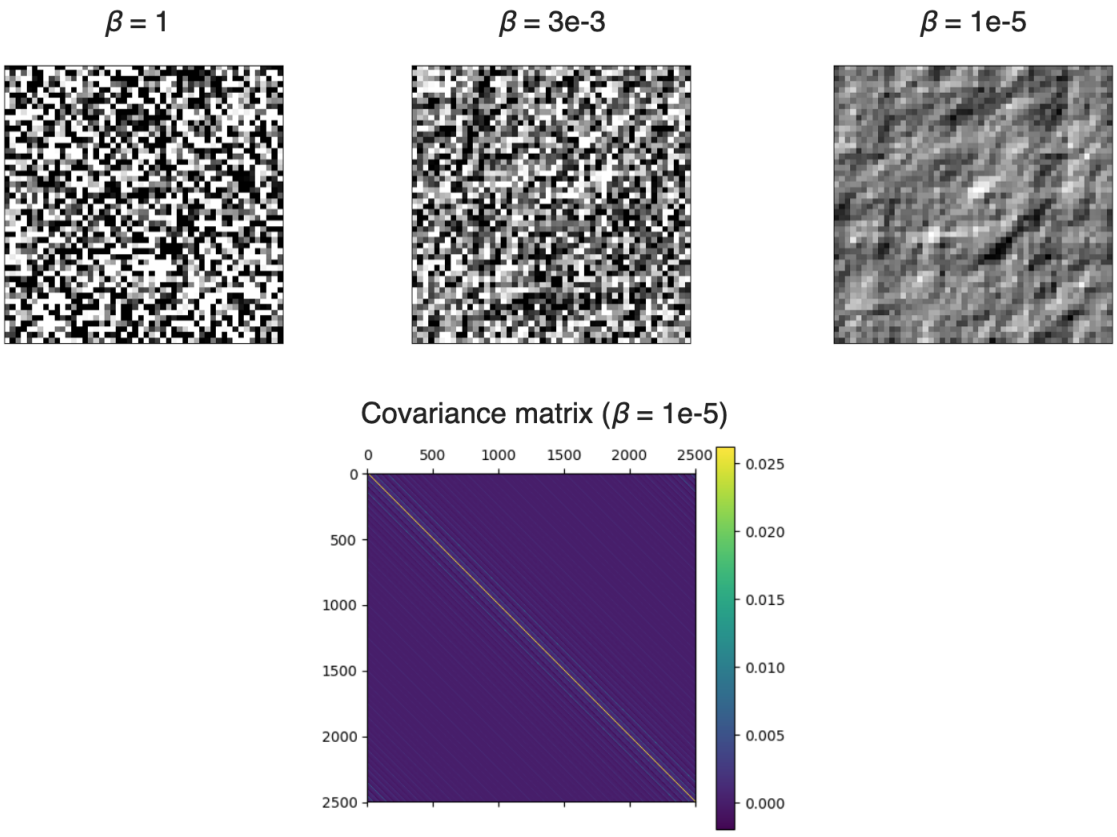

Figure 2-5: Top row: Correlated 50×50 scenes with three different values of β. $\beta = 1$ implies an IID scene, with increasing correlation as β approaches 0. On bottom: the covariance matrix with $\beta = 10^{-5}$. Note that the covariance matrix is 2500×2500, since it describes the covariance of each of the 2500 scene pixels with each other pixel. The pattern of banding that you see depends on how we choose to flatten the 50×50 scene array into a 2500-entry vector; here, the scene is flattened in reading order.

rise to the $1/n$ factor.

(Shot noise): This includes measurement noise that depends on the contribution due to the scene of interest. This results in additive Gaussian noise of variance $\rho \cdot \frac{J}{n}$ (proportional to the net power of light that goes through the aperture).

Thermal noise should be more important in passive non-line-of-sight imaging applications using accidental cameras (in other words, the applications described in Chapter 3) because in that application, the bulk of the light reaching the observation will generally come from sources that aren't the scene of interest, like overhead lighting or sunlight.

Shot noise should be more important in designer-camera applications using coded apertures (in other words, the applications most relevant to the considerations described in Chapter 2) because in those applications, the camera will presumably be designed in such a way as to prevent glare.

Both of these sources of noise are in reality captured by a Poisson distribution, since that's the way light behaves in real-world scenarios. Fortunately, the limit of a Poisson distribution as the number of photons gets very large is a Gaussian, which is much more easily modeled. This approximation is extremely close to reality in the applications we're interested in, which are passive-imaging applications with plenty of light. In super-low-light applications, however, such as active-imaging scenarios where the scene is in perfect darkness except for light introduced by the experimenter through a laser, this modeling issue can become important.

Now that we've established the noise model, we can finally write down the equation relating the scene to the observation.

$$y = Ax + \eta$$

$$x \sim \mathcal{N}(\mu \mathbf{1}, Q)$$

$$\eta \sim \mathcal{N}(0, (W + \rho \cdot J)/n)$$

We'll leave Q ambiguous for now, and talk about it on a case-by-case basis depending on the application. $\mu = J/n$ as described earlier. J is the total radiance

of the scene, whereas W is a parameter that describes the level of glare (the scene-independent noise).

2.3.4 Mutual Information

Mutual information. The mutual information (MI) between the measurements $y_j, j \in [n]$ and the unknowns $f_i, i \in [1, n]$ of the imaging problem is given as $\mathcal{I} = \log\det\left(\frac{1}{\sigma^2}\widetilde{\mathbf{A}}\mathbf{Q}\widetilde{\mathbf{A}}^T + \mathbf{I}\right)$, where the noise variance $\sigma^2 = (W + \rho \cdot J)/n$.

2.4 High SNR, IID scene, Occluding mask

In this section, I will go into great detail about a regime that appears unphysical, but gives us a lot of insight into a variety of different important regimes. It also has important mathematical implications.

Consider the mutual information equation from the previous section:

$\mathcal{I} = \log\det\left(\frac{1}{\sigma^2}\widetilde{\mathbf{A}}\mathbf{Q}\widetilde{\mathbf{A}}^T + \mathbf{I}\right)$

Suppose we make the following assumptions:

1. The scene is IID, $Q = kI$.
2. The SNR is very good, $\sigma \ll k$, so we can ignore the identity term.
3. The intermediate frame only occludes light or lets it through; it doesn't redirect the light.
4. The far-field assumption applies. This point and the previous one let us assume that the transfer matrix $\widetilde{\mathbf{A}}$ is a multiple of a binary-valued Toeplitz matrix.

Suppose now that we want to find the best possible intermediate frame under these conditions, i.e. we want to find the best possible transfer matrix that satisfies the constraints above.

What transfer matrix maximizes the mutual information? Naturally, it will be whichever transfer matrix maximizes $\log\det\left(\frac{1}{\sigma^2}\widetilde{\mathbf{A}}\mathbf{Q}\widetilde{\mathbf{A}}^T + \mathbf{I}\right)$, which given our assumptions is equivalent to maximizing the determinant of $\widetilde{\mathbf{A}}^T\widetilde{\mathbf{A}}$. This corresponds to

maximizing the product of the norms of the transfer matrix's singular values, since each eigenvalue of $\widetilde{\mathbf{A}}^T\widetilde{\mathbf{A}}$ corresponds to the norm squared of one of the eigenvalues of $\widetilde{\mathbf{A}}$.

If we further assume that $\widetilde{\mathbf{A}}$ is circulant, not just Toeplitz, then that tells us that in fact the eigenvalues and singular values of $\widetilde{\mathbf{A}}$ have the same norm. This is a convenient assumption that doesn't necessarily match reality. Under which real-world conditions will the transfer matrix actually be circulant rather than Toeplitz? This is somewhat unintuitive, but it corresponds to the scenario in which the occluding pattern of the intermediate frame repeats itself once. Once is enough! See Figure **??** for a visual explanation of why this is.

Assuming that the transfer matrix is circulant, not just Toeplitz, is tremendously convenient. It means that we can compute the mutual information between the scene and the observation extremely efficiently, since the eigenvalues λ_i are given by the Fourier transform of the first row of the transfer matrix, for which the time to compute is log-linear in n (as opposed to $O(n^3)$ for a general determinant). And since $|\lambda_i| = |\sigma_i|$, that gives us all the information we need to compute $\log\det(\widetilde{\mathbf{A}}\widetilde{\mathbf{A}}^T)$.

But realistically speaking, can we restrict ourselves just to circulant transfer matrices rather than Toeplitz ones? After all, occluders that give rise to that kind of transfer matrix make up only a very small fraction of all possible occluders. The answer is that it depends on what you want, but if you're only concerned with finding the *best* possible occluder, restricting your attention to circulant transfer matrices costs you very little. Here's why.

2.4.1 Hadamard's Bound

The point of this section is to justify the following bound on all $\{0,1\}$ matrices B. If this doesn't interest you, skip to the next section.

$$|\det B| =\leqslant 2^{-n}(n+1)^{(n+1)/2}, \tag{2.1}$$

By a *binary* matrix we mean a matrix whose elements are in one of the sets

$S_{01} := \{0, 1\}$ or $S_{\pm 1} := \{-1, 1\}$. It will be clear from the context which of these two cases is being considered. A *binary circulant* is a circulant matrix whose elements are in S_{01} or $S_{\pm 1}$.

There is a natural correspondence between the integers $\{0, 1, \ldots 2^n - 1\}$ and the binary circulant matrices of order n. If $N \in \{0, 1, \ldots, 2^n - 1\}$ has the representation

$$N = \sum_{j=0}^{n-1} 2^{n-1-j} b_j,$$

so may be written in binary as $b_0 \ldots b_{n-1}$, we associate N with $\mathrm{circ}(a_0, \ldots, a_{n-1})$, where $a_j = b_j$ in the case of S_{01}, and $a_j = 2b_j - 1$ in the case of $S_{\pm 1}$.

The *maximal determinant problem* is concerned with the maximal value of $|\det A|$ for an $n \times n$ binary matrix A. The *Hadamard bound* [**?**] states that, in the case of binary matrices A over $\{\pm 1\}$, we have

$$|\det A| \leqslant n^{n/2}. \tag{2.2}$$

Moreover, Hadamard's inequality is sharp for infinitely many n, for example powers of two or n of the form $q+1$ where q is a prime power and $q \equiv 3 \pmod 4$ (Paley [**?**]).

There is a well-known connection between the determinants of $\{0, 1\}$-matrices of order n and $\{\pm 1\}$-matrices of order $n + 1$. This implies that an $(n + 1) \times (n + 1)$ $\{\pm 1\}$-matrix always has determinant divisible by 2^n. See [**?**] for details. We give an example with $n = 3$, starting with an $n \times n$ binary matrix B and ending with an $(n + 1) \times (n + 1)$ $\{\pm 1\}$-matrix A, with $\det A = 2^n \det(B)$.

$$B = \begin{pmatrix} 1 & 0 & 1 \\ 1 & 1 & 0 \\ 0 & 1 & 1 \end{pmatrix} \xrightarrow{\text{double}} \begin{pmatrix} 2 & 0 & 2 \\ 2 & 2 & 0 \\ 0 & 2 & 2 \end{pmatrix}$$

$$\overset{\text{border}}{\longrightarrow} \begin{pmatrix} 1 & 1 & 1 & 1 \\ 0 & 2 & 0 & 2 \\ 0 & 2 & 2 & 0 \\ 0 & 0 & 2 & 2 \end{pmatrix} \overset{\substack{\text{subtract} \\ \longrightarrow \\ \text{first row}}}{} \begin{pmatrix} 1 & 1 & 1 & 1 \\ -1 & 1 & -1 & 1 \\ -1 & 1 & 1 & -1 \\ -1 & -1 & 1 & 1 \end{pmatrix} = A.$$

The doubling step is the only step where the determinant changes, and there it is multiplied by 2^n.

Thus, Hadamard's bound (2.2) gives the bound

$$|\det B| = 2^{-n} |\det A| \leqslant 2^{-n}(n+1)^{(n+1)/2}, \tag{2.3}$$

which applies for all $\{0,1\}$-matrices B of order n. We shall refer to both (2.2) and (2.3) as *Hadamard's inequality*, since it will be clear from the context which inequality is intended.[5]

2.4.2 Binary Circulants Achieving Hadamard's Bound

Now we get to the reason that, if you're only concerned with finding the *best* possible occluder, restricting your attention to circulant transfer matrices costs you very little. The reason is that there are several constructions for binary circulant matrices that achieve Hadamard's bound—this *despite* the fact that Hadamard's bound is general for all binary matrices, not just circulant ones! Please take a moment to reflect on how lucky it is that among the binary circulant matrices, which comprise a tiny subset of all binary matrices that, some of those binary circulant matrices achieve determinants as large as any from *all* binary matrices of the same size. I'll call these remarkable binary circulants "determinant-maximizing binary circulants," or DMBCs.

There are four known constructions for DMBCs. All four of these constructions yield a matrix whose eigenvalues are all equal, save for the first; the first eigenvalue has a value of $(n+1)/2$, and every other eigenvalue has a value of $\sqrt{(n+1)/2}$. The

[5] In fact, Hadamard in [?] proved a more general inequality than (2.2), and as far as we are aware he never stated (2.3) explicitly. A simple proof of (2.2) is given by Cameron [?].

dot product of any pair of rows in a DMBC from one of these four constructions is $(n+1)/4$. In each construction, there are $(n+1)/2$ 1s and $(n-1)/2$ -1s. It follows from that last sentence that if you take one of these constructions and replace all the 0s with -1s to yield a $\{1,-1\}$ matrix, the dot product of any pair of rows will be -1.

Thanks to this last point, DMBCs have a close relationship to Hadamard matrices. Hadamard matrices are $\{1,-1\}$ matrices (not necessarily circulant) for which every pair of rows is orthogonal, that is, the dot product of any pair of rows is 0. (The same is true of pairs of columns.) Any size-n DMBC from one of these four constructions can be easily adapted to create a size-$(n+1)$ Hadamard matrix as follows: replace all the 0s with -1s in the DMBC, and then add a first row and a first column of all -1s. The dot product of the first row with any other row will be 0 (because every other but the first is exactly half 1s and half -1s). The dot product of every row other than the first with any other row other than the first will also be 0 (because the dot product of each pair of rows before adding the extra row and column was -1, and then adding the extra column adds an extra 1 to the dot product). Hence each size-n DMBC yields a size-$(n+1)$ Hadamard matrix.

Hadamard matrices of this kind are known in the literature as "Hadamard matrices with circulant core," for obvious reasons. Now I will go into a little bit more detail about the various constructions.

Theorem 1 (Hadamard circulant core construction)**.** *A Hadamard matrix of order $n+1$ with circulant core of order n exists if*

(1) $n \equiv 3 \pmod 4$ *is a prime;*

(2) $n = p(p+2)$*, where p and $p+2$ are prime;*

(3) $n = 2^k - 1$*, where k is a positive integer; or*

(4) $n = 4k^2 + 27$*, where k is a positive integer and n is a prime.*

Proof. Case (1) is due to Paley [**?**]; case (2) is due to Stanton and Sprott [**?**] and also Whiteman [**?**]; case (3) is due to Singer [**?**]; and case (4) is due to Hall [**?**, Theorem 2.2]. □

Hall [**?**, p. 980] remarks that case (4) is subsumed by case (1), since $4k^2 + 27 \equiv 3 \pmod 4$, but we mention case (4) since Hall's construction is different from that of Paley.

We do not know if the list given by Theorem 1 is exhaustive. The computational results given in Tables **??**–**??** show that, for $1 \leqslant n \leqslant 52$, only those n given by Theorem 1 can provide a Hadamard matrix of order $n+1$ with a circulant core. Also, a circulant $\{0, 1\}$-matrix of order $n \leqslant 52$ can achieve the upper bound (**??**) if and only if $n \leqslant 4$ or n satisfies condition (1), (2) or (3) of Theorem 1.

This gives us the four known constructions for DMBCs. Note that the fourth construction is completely redundant with the first, since any prime n such that $n = 4k^2 + 27$ where k is a positive integer is guaranteed to also be prime and congruent to 3 mod 4! It is only considered a separate construction because it yields an additional DMBC beyond the one given by the first construction (that isn't a trivial transformation). The fourth construction is therefore of no additional practical value to us: we can't use it to create a mask that images at a given level of resolution that we couldn't already. It's quite interesting mathematically, but doesn't help us solve an imaging problem.

It's worth giving more detail about the first construction, since it's by far the most common one over the real numbers; there are many more primes congruent to 3 mod 4 than there are powers of 2 or products of twin primes! Indeed, it's common enough that no matter what level of resolution you need, there will be a reasonably suitable mask at a nearby resolution level, thanks to the first construction.

The first construction, due to Paley, is as follows:

If n is prime and congruent to 3 mod 4:

$$x_i = \begin{cases} 1 & \text{if } \left(\frac{i}{n}\right) = 0 \text{ or } 1 \\ 0 & \text{otherwise} \end{cases}$$

Here, $\left(\frac{i}{n}\right)$ is the Legendre symbol. It's equal to 0 is a multiple of n, and is otherwise equal to 1 if i is a quadratic residue (meaning a perfect square) modulo p and -1 if

not. It's very easily computed, since by Euler's criterion, we have, for any a and any prime p:

$$\left(\frac{a}{p}\right) \equiv a^{(p-1)/2} \mod p$$

Figure 2-6 shows the first few sequences of the Paley construction. As you can see, it has a very "random-looking" appearance. Of course, the construction is very much non-random; what gives it that appearance, though, is its non-self-repeating character. All four constructions, in fact, try to repeat themselves as little as possible. That's not surprising from the point of view of wanting to keep the sequence's Fourier spectrum flat, of course. But the way I like to think of it from an imaging point of view is that these sequences try and make the different possible shadows cast by a light source in a variety of different locations as different as possible from each other. A light source at each possible point in the (implicitly planar) scene will yield a different rotation of the occluding sequence, so the best sequences for distinguishing light sources at different locations will be sequences that are orthogonal to their own rotations. See Figure 2-7 for a visual explanation of this phenomenon.

In any event, because DMBCs achieve the maximal possible mutual information of any binary matrix of their size, the fact that we restricted our attention to circulant matrices rather than considering all possible Toeplitz matrices doesn't matter, assuming the value of n we're using admits the existence of a DMBC. We therefore know that the once-repeating occluder suggested by that DMBC outperforms all other possible occluding intermediate frames, including ones that don't repeat themslves.

Why is this useful, if the notion of an IID scene doesn't make sense, as we explained in the previous section? After all, these sequences are only optimal assuming an IID scene, and each different value of n yields a qualitatively difference scene model. How can we know which of these non-repeating sequences to apply in real life?

The answer is that even if "IID scenes" with different values of n are qualitatively different from each other, that doesn't mean that each one doesn't describe a reasonable approximation of reality. Each different value of n can be thought of as describing

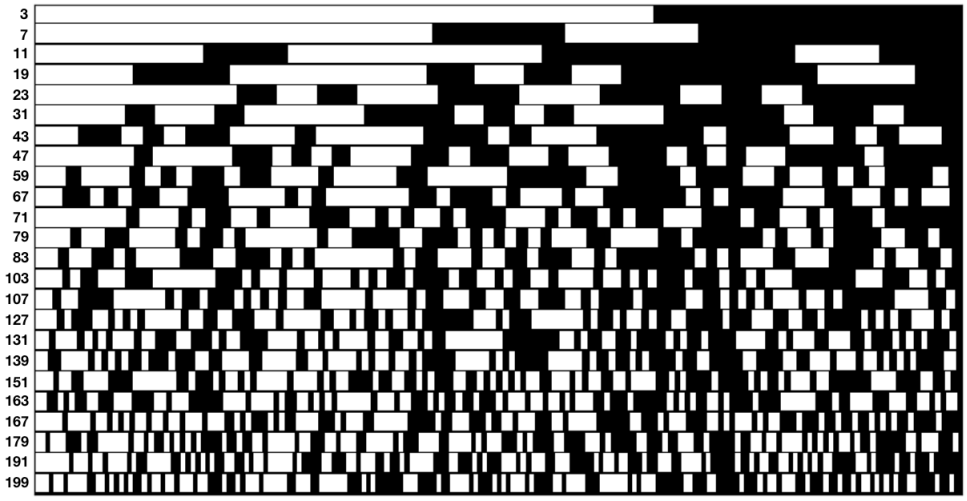

Figure 2-6: These are the first few Paley sequences, i.e. on-off patterns whose spectrum is flat and that yield a DMBC (determinant-maximizing binary circulant) when used as the first row of a circulant matrix. On the left is n, the number of on/off chunks used. Note that for a Paley sequence to exist, n must be prime and congruent to 3 mod 4.

a different model, with lower values of n describing scenes with fewer "effective pixels" and higher values describing scenes with more "effective pixels." What do I mean by the number of "effective pixels" that a scene has? Well, roughly speaking, it's the number of pixels you need to get a reasonable view of the scene; you can think of a 144p video as having 144 effective pixels, even if more pixels than that are used to display it on your screen. More correlated scenes will have fewer effective pixels, and less correlated scenes will have more; having a lower SNR will also mean you have fewer effective pixels, and a higher SNR will mean you have more.

Figure 2-15 is a plot of the approximate number of effective pixels in the system, as a function of the SNR and β (i.e. the level of correlation in the scene).

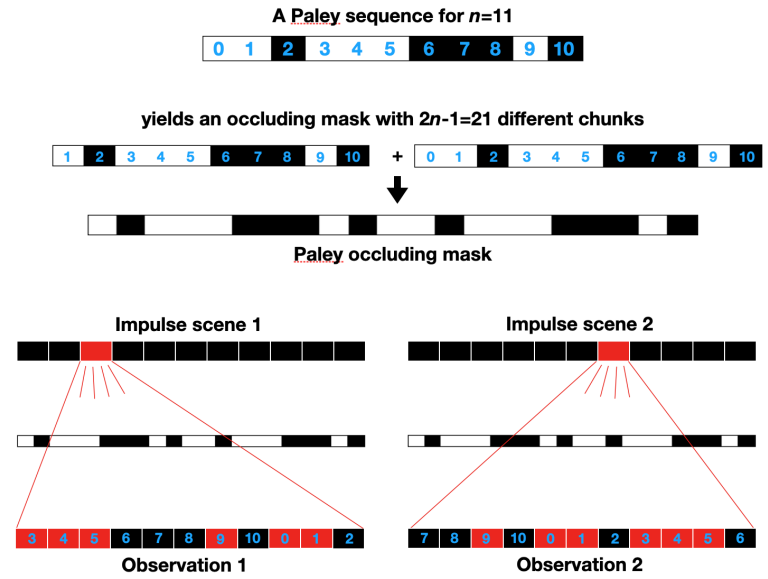

Figure 2-7: A visual explanation of Paley sequences, the "optimal" occluding masks that be constructed from them, and the transfer matrices associated with those masks. Top: we consider the Paley construction applied to the case $n = 11$. The paley construction gives us a binary sequence, with 1's (white, or "on") element i of the sequence if i is 0 or a quadratic residue modulo n, and 0's (black, or "off") for elements i of the sequence if i is not a quadratic residue modulo n. From this sequence we get an occluding mask, which consists of the sequence twice; every element is repeated exactly once except for the 0 element, which is in the center. Given the far-field assumption and assuming the occluder is halfway in between observation and scene, an impulse scene will cast a shadow that corresponds to half the occluder, which is some rotation of the original Paley sequence. Bottom: sequences given by the Paley construction (as well as any other flat sequence) are as different as possible from their own rotations; this means that depending on where the impulse light source is in the scene, the cast shadows will be as different as possible. This makes reconstructing the location of a point light source, given a cast shadow, as easy as possible.

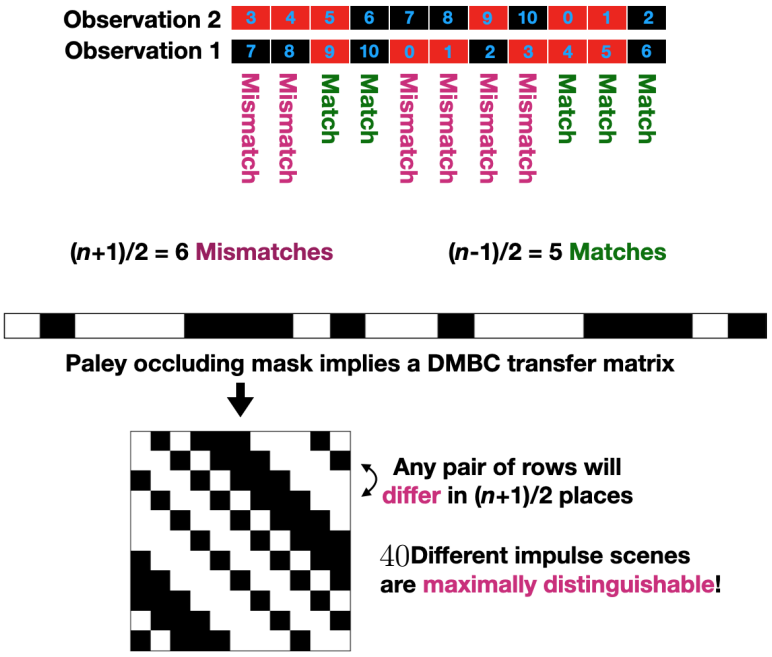

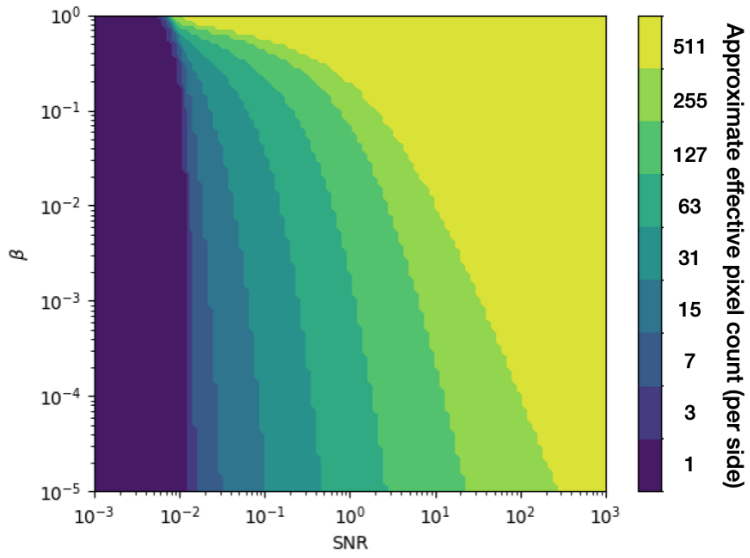

Figure 2-9: Top: the approximate effective pixel count of scenes generated with a given level of correlation (β) and under a given signal-to-noise ratio (SNR). As expected, more correlated scenes and noisier scenes both have fewer effective pixels. Note, however, that even highly correlated scenes can have high effective pixel counts if the SNR is high enough, but if the SNR is low enough the scene will always have a low effective pixel count. Effective pixel count was estimated by choosing which of the nine spectrally-flat masks shown on bottom yielded the highest mutual information. Bottom: masks corresponding to each of the effective scene pixel counts. Note that these masks repeat themselves once in each dimension, so each mask is $2n-1 \times 2n-1$ if the effective pixel count is n. This is due to the phenomenon described in Figure **??**.

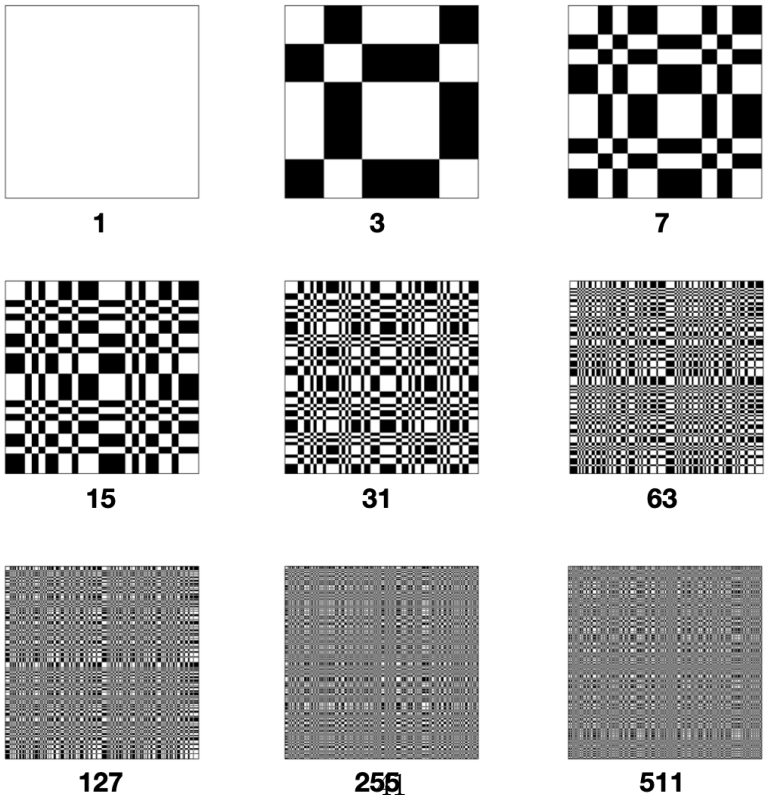

2.5 Varying the distance between observation, occluder, and scene

We continue examining each of the idealized model's assumptions one after the other. Next on the docket is the assumption that the occluder lies exactly halfway in between the scene and observation plane. This was a tremenously convenient assumption because it allowed us to assume that the occluder's transfer matrix had Toeplitz structure. But in the real world, the assumption is completely unrealistic. In a designer-mask camera application, the occluder will presumably be much closer to the camera's photosensitive material than to the scene, and even in an accidental-camera application, we can't assume that the occluder will be exactly halfway between the wall we're looking at and whatever it is we're trying to image. So let's try removing the assumption and seeing what happens. Note that we'll still be assuming that scene and occluder are both planar—we'll get to that eventually, but not yet. And we're still using the far-field assumption—meaning that regardless of what we are taking the *relative* distances of the occluder to the scene and observation to be, we are always assuming that the distance between scene and observation to be much bigger than the size of the scene or observation.

What exactly is it about an occluder halfway between the scene and observation that gives us Toeplitz transfer matrices? The answer is that when the occluder is halfway bewteen the scene and observation, the shadow cast by a moving light source will move at exactly the speed the light source is moving, but in the opposite direction. Try holding a flashlight (such as one from a smartphone) with your right hand, illuminating a table or a wall, and then hold your left hand halfway in between the flashlight and the table. (I encourage you to actually do this!) Keep your left hand steady, and then move the flashlight around. You can see that your hand's shadow moves at the same speed your flashlight does, and in the opposite direction.

Now try varying the height of your left hand relative to the table. What happens to the speed of your hand's shadow relative to the speed at which you move the flashlight? The answer is that when your hand is closer to the table than to the

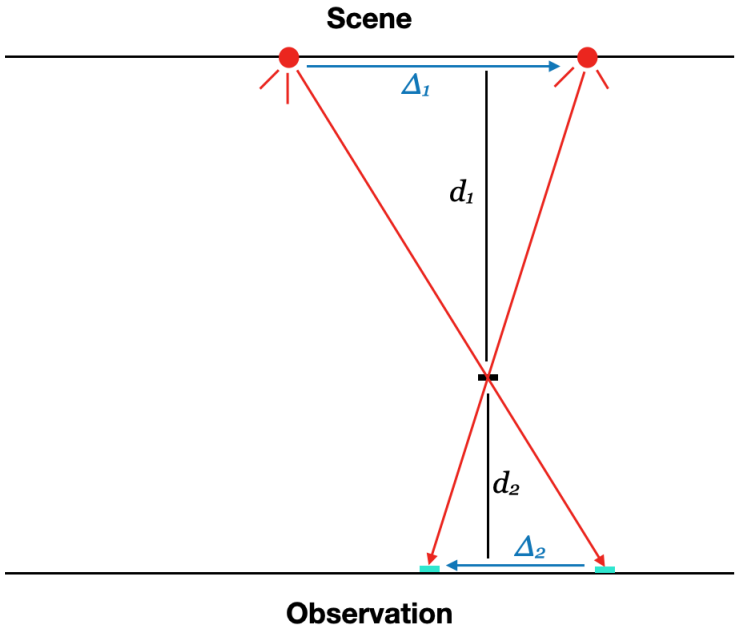

Figure 2-11: A simple layout that explains the phenomenon whereby the relative speeds of a light source and its shadow are given by the relative distances of the scene and the observation to the occluder. Suppose we have a pinspeck occluder, and a light source that moves by an amount Δ_1 to the right. If we suppose that its shadow moves by an amount Δ_2 to the left, and that the occluder has a perpendicular distance d_1 from the scene and d_2 from the observation, then the fact that the top and bottom triangles are similar tells us that $\Delta_1/\Delta_2 = d_1/d_2$.

flashlight, your hand's shadow will move slower than the flashlight; and when your hand is closer to the flashlight than to the table, your hand's shadow will move faster than the flashlight. (Of course, your hand's shadow will always in the opposite direction from the shadow—that part won't change.)

In fact, to be more precise, the "speed multiplier" that your hand's shadow gets relative to the flashlight—that is, your hand's shadow's speed divided by the flashlight's speed—is the same as the distance between your hand and the table divided by the distance between your hand and the flashlight. Figure 2-11 gives a visual explanation of this phenomenon.

This "speed multiplier" conceit is crucial to understanding how varying the occluder's depth warps the resulting transfer matrix. Remember that each column of the transfer matrix tells us what the observation will look like in response to a point

light source at each different location in the scene. If we imagine, then, a point light source moving at a constant speed of 1 space-unit per time-unit across the scene, then we can imagine the transfer matrix as a movie of the observation plane while that happens, with each column of the transfer matrix being one frame of that movie.

When the occluder is halfway in between the scene and observation plane, we know exactly what that movie should look like: the shadow should move at the same speed as the point light source. That is, it should move at a speed of 1 space-unit (1 "bin," or $1/n$) per time unit (1 "frame," or column of the transfer matrix), assuming we discretize the scene and the observation plane equally finely.

It's for this reason that the occluder being halfway between the scene and observation gives us the perfect, constant diagonals that characterize a Toeplitz matrix. Compare a column of the transfer matrix to the column adjacent to it, and you should see a copy of that column, but shifted by one row.

What if we continue to imagine that the transfer matrix is a movie of the shadow cast by a point light source moving a constant speed of 1 space-unit per time-unit—but now we supposed that the occluder was twice as close to the scene as it was to the observation plane? We know from Figure 2-11 that that means that the shadow must move at a speed of 2 space-units per time-unit. Therefore, on the transfer matrix, moving one column (time-unit) to the right will cause the shadow to shift two rows (space-units) down. (Remember that we are sticking to our convention of labeling the observation plane right-to-left instead of left-to-right, as explained in Section **??**—if we weren't, that would cause the shadow to shift two rows *up*!)

Similarly, if the occluder was twice as close to the observation plane as to the scene, the shadow would move at a speed of 0.5 space-units per time-unit. And if the occluder was right up against the observation plane, the shadow wouldn't move at all—and if the occluder was right up against the scene, there would be no shadow! Figure 2-12 shows some example transfer matrices for each of these scenarios.

If you look carefully at Figure 2-12—in particular the second and fourth setups, in which the occluder is a quarter or three-quarters of the way to the scene—you'll see that the transfer matrix isn't perfectly binary, like some of the previous transfer

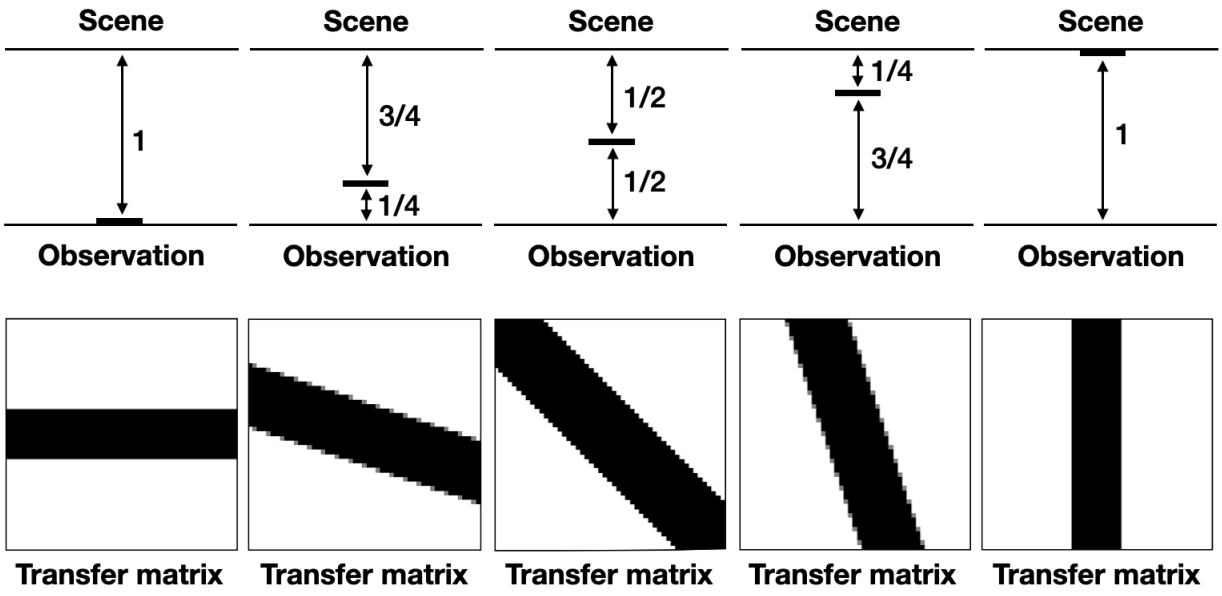

Figure 2-12: Top row: five different scenarios with the occluder at five different depths. Bottom row: the transfer matrices corresponding to each different scenario.

matrices we've looked at. It contains a few entries that lie between 0 and 1. This isn't for any legitimate reason, like a partially opaque occluder; this is purely a modeling issue. It has to do with the fact that, in order to approximate the scene and observation, we've partitioned them both into discrete chunks. If they were both perfectly continuous, their transfer matrices would both be completely binary, as we'd hope to see. The problem is, though, this isn't quite a issue we can wish away by appealing to what happens in the limit as our discretization becomes finer and finer: even if our discretization was extremely fine, the absolute number of nonbinary elements in our transfer matrix wouldn't shrink; in fact, it would grow! Granted, the *fraction* of nonbinary elements in our transfer matrix would shrink, but even that isn't true if we also suppose that our occluders become increasingly complex (with more and more interfaces between occluding and not-occluding). So our model remains annoyingly unfaithful to reality even when we discretize very finely.

Why is having nonbinary elements in our transfer matrix a problem? Beyond the simple fact that it doesn't accurately describe reality, it will result in us underestimating the mutual information of setups where the occluder is not exactly halfway

in between scene and occluder. This is because nonbinary elements in the transfer matrix (or the occluder, for that reason!) tend to lead to low mutual information, for reasons described in more detail in Section **??**. This effect gets exacerbated when the occluder is just a little bit off from being halfway in between the scene and occluder. For example, suppose the occluder is 5/11 of the way between the observation and the scene; the resulting transfer matrix will have its diagonals of constancy be terribly skew to the diagonals of the matrix, resulting in a lot of nonbinary elements.

Fortunately, there's an easy solution to this modeling issue, and it doesn't require us to treat everything as fully continuous. The key fact here is that we can relate the eigenvalues of the Gram matrix $AQA^T + I$ derived from the true, continuous transfer matrix A (which is square) to the eigenvalues of the equivalent Gram matrix $A_rQA^T + I$ derived from a rectangular version A_r of the transfer matrix A.

The way we obtain A_r from A is simply to "stretch" the matrix A (whose lines of constancy lie skew to the diagonals of the transfer matrix) until we get a version whose diagonals align with the diagonals of the transfer matrix. Figure 2-13 shows how this works.

To figure out how much to rescale in response to the stretching of the matrix, it is instructive to consider the all-ones transfer matrix (corresponding to no occlusion in the far-field limit). This is a helpful transfer matrix for gaining intuitions about these setups in general; it will be very helpful here.

Because the all-ones transfer matrix corresponds to no occlusion, we can equivalently posit the occluder "plane" to be at any depth. Let's imagine it's $w/(w+h)$ of the way to the scene (meaning that if the distance between scene and observation is d, then the distance between the occluder and the scene is $hd/(w+h)$ and the distance between the occluder and the observation is $wd/(w+h)$.) As Figure 2-13 shows us, that tells us that if the true transfer matrix has a width-to-height ratio of 1:1, the stretched transfer matrix will have a width-to-height ratio of w:h.

This has two impacts on the value of the determinant of $A^TQA + I$. The first is that $A^TQA + I$ is a bigger matrix, which will cause the value of the determinant to increase. The second is that each entry of A^TQA is smaller, because A^T is narrower

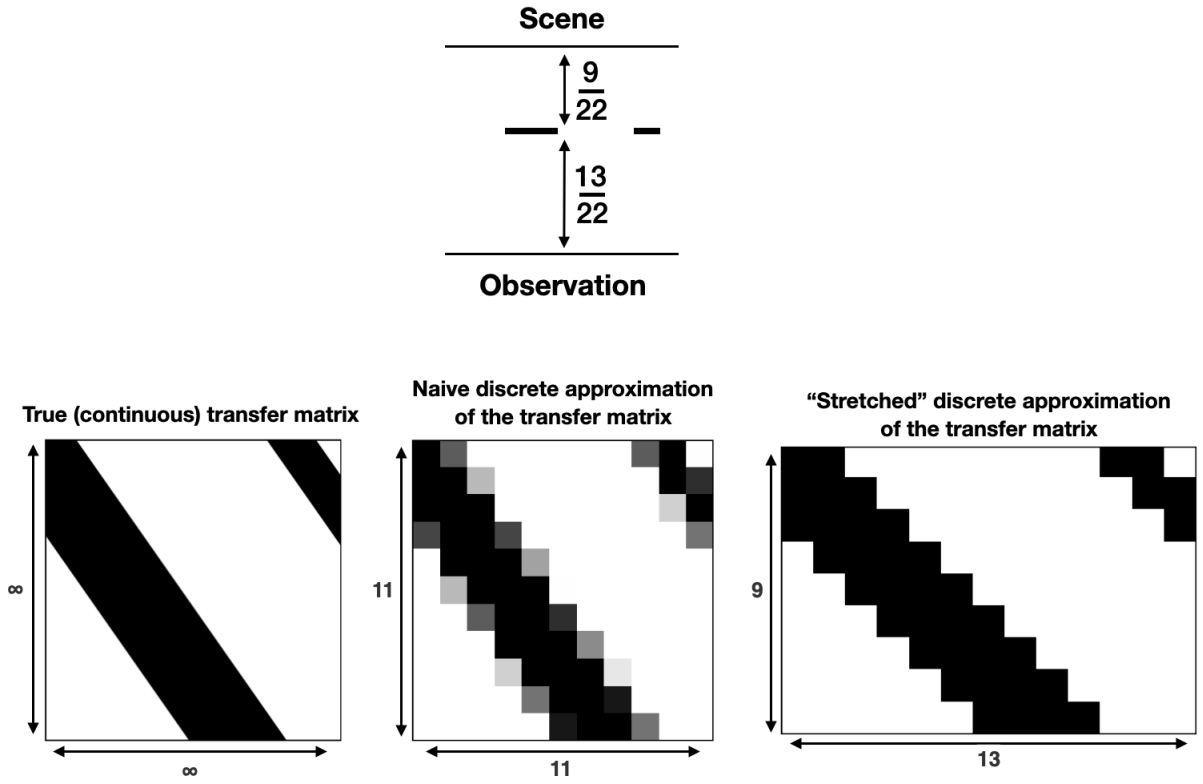

Figure 2-13: Top: a setup with a planar occluder not halfway in between the scene and the observation. If we take the distance between the scene and observation to be d, then the distance between the scene and occluder is $\frac{9}{22}d$ and the distance between the occluder and observation is $\frac{13}{22}d$. We take a discretization level of $n = 11$ (so for computational reasons, we are modeling the scene and observation as vectors of $n = 11$ constant entries, and the occluder as a vector of $2n-1 = 21$ constant entries). Bottom left: the true, continuous transfer matrix. Bottom middle: the naive discrete 11×11 approximation of the transfer matrix, using averaging to produce nonbinary elements. Bottom right: the "stretched" 9×13 approximation of the transfer matrix, yielding a rectangular matrix with Toeplitz structure and only binary elements.

and A is shorter; this will cause the value of the determinant to decrease. To rectify the first effect, it is necessary to rescale A^TQA by a factor of n^2/w^2. To rectify the second, it is necessary to rescale each eigenvalue of the A^TQA by a factor of n/h (so that taking the determinant of $A^TQA + I$ means taking the product $\prod_i 1 + \lambda_i(n/h)$), where λ_i denotes the i^{th} eigenvalue of the (rescaled) matrix A^TQA.

To be a bit more concrete: recall our original formula for computing the mutual information of an occlusion-based system. Let A be the transfer matrix of the system, scaled to be binary-valued. Now let A_r be the rectangular equivalent of that transfer matrix, stretched so that the diagonals of constancy are the actual diagonals of the matrix. Ordinarily, we would write (as we described in Section **??**) that the mutual information $\mathcal{I}$ is given by:

$$\mathcal{I} = \det(\sigma A^TQ(n)A/n^2 + I) = \prod_i (1 + \lambda_i(\sigma A^TQ(n)A/n^2))$$

where $Q(n)$ is the covariance matrix of the scene, σ is the signal-to-noise ratio, and $\lambda_i(A^TQA)$ denotes the i^{th} eigenvalue of A^TQA.

Instead of taking A to be a square matrix with diagonals of constancy that are skew to the actual diagonals of the matrix, we stretch it so that its width to height ratio is w:h. Let's take its dimensions to be $w \times h$. Call this new, stretched matrix A_r. Now we can write:

$$\mathcal{I} = \prod_i (1 + \frac{n}{h}\lambda_i(\sigma A_r^TQ(w)A_r/w^2))$$

In the limit of continuous transfer matrices, these two formulations are perfectly equivalent. But when we approximate the continuous transfer matrix by using a discrete matrix, the difference between these two "equivalent" formulations can be dramatic—and, of course, it's the rectangular formulation that gets closer to the truth. See Figure 2-14 for a side-by-side comparison.

This trick lets us faithfully represent systems involving occluders at $2n-1$ different depths, where n is the level of discretization of the scene. This is tremendously convenient! It lets us do an accurate study of how much having occluders not exactly

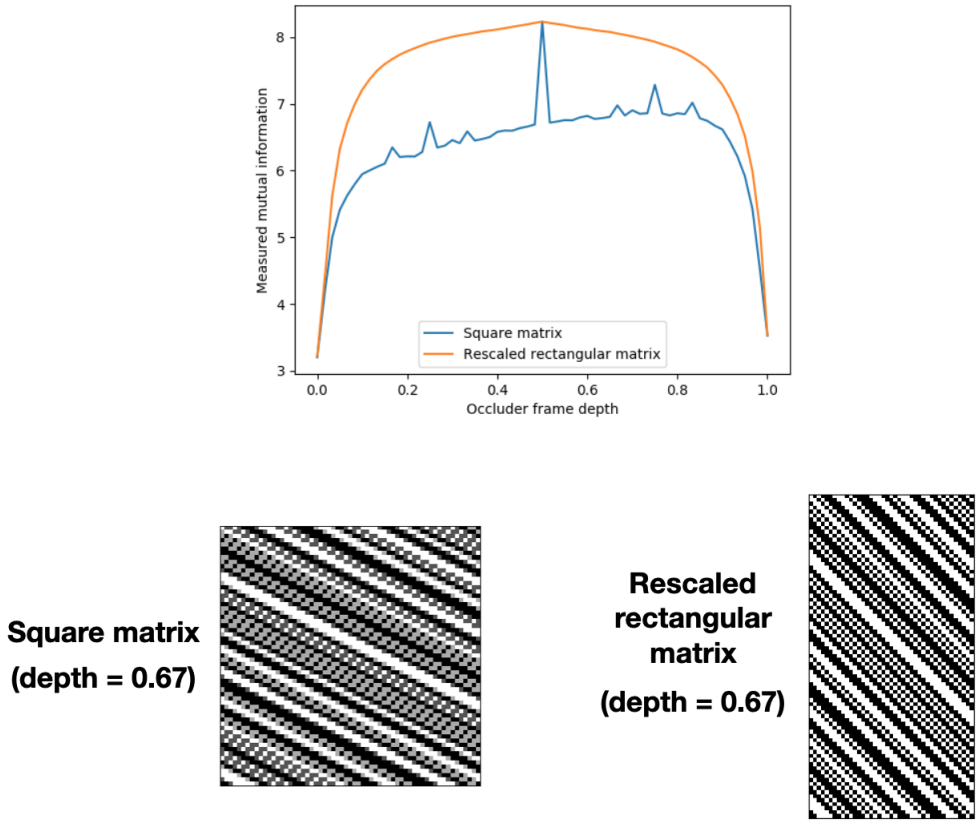

Figure 2-14: A comparison of observed mutual information using either a square matrix with non-binary averaged values, or a stretched rectangular matrix, appropriately rescaled. In this example, $n = 61$. It is apparent that the effect of averaging values in the square matrix leads to a dramatic (and artifactual) decrease in the observed mutual information, as well as artifacts at depths that make there be fewer nonbinary values in the square matrix.

halfway in between the scene and observation harms performance. We know, of course, that it must: DMBCs have diagonals of constancy in line with the matrix's diagonals, and skewing those diagonals decreases the rank of the resulting transfer matrix! But by how much is an interesting question. Figure **??** gives an answer. Just like Figure 2-15, it helps us estimate the effective pixel count of the setups involving occluders at different depths. As expected, moving the occluder away from the halfway point reduces the setup's effective pixel count—but interestingly, the effective pixel count doesn't change much until the occluder is moved far from the halfway point (e.g. 10% or 90% of the way to the scene). This tells us that using a good occluder matters a lot more than making sure it's exactly halfway between scene and observation, for the purposes of maximizing mutual information.

2.6 Near-field scenes

Next, we tackle the question of what happens to our analysis when we discard the far-field assumption. Real scenes, after all, don't lie infinitely far away from our cameras. And though we saw in Section **??** that the far-field assumption is deceptively robust, because of the quadratic dependence on distance in the illumination function (see Equation **??**), that doesn't mean it's *right*. So let's analyze our standard setup more carefully, without taking the far-field assumption.

Way back in Section **??**, we decided to use a reversed labeling system, such that the scene vectors were ordered left-to-right (as normal) but the observation vectors were ordered right-to-left. This was so that the diagonals of constancy of the resulting transfer matrices would go from upper-left to lower-right. This lets us work with the more intuitive, well-studied circulant and Toeplitz matrices, rather than their less well-known and -studied Hankel cousins. Of course, in the end, it doesn't matter what labeling scheme we use: the math must work out the same in either case. However, this reverse labeling was more convenient in the previous sections.

In this section, to avoid confusion, we'll stick with the same convention as we used in previous sections. Unfortunately, though, in this section, it won't buy us

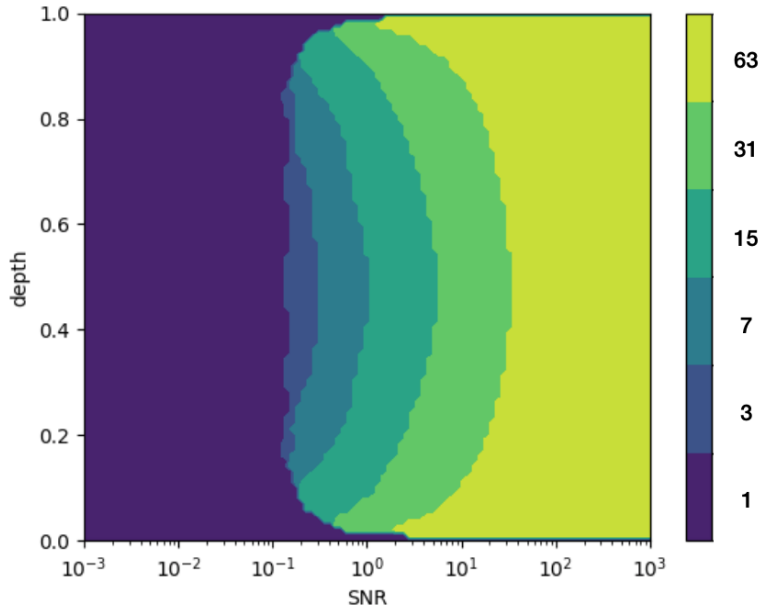

Figure 2-15: Top: the approximate effective pixel count of scenes generated at different occluder depths. As expected, when the occluder is near the observation plane or the scene, it reduces the number of effective pixels. Here the scene correlation $\beta = 10^{-3}$. Bottom: masks corresponding to each of the effective scene pixel counts. Note that these masks repeat themselves once in each dimension, so each mask is $2n-1 \times 2n-1$ if the effective pixel count is n. This is due to the phenomenon described in Figure **??**.

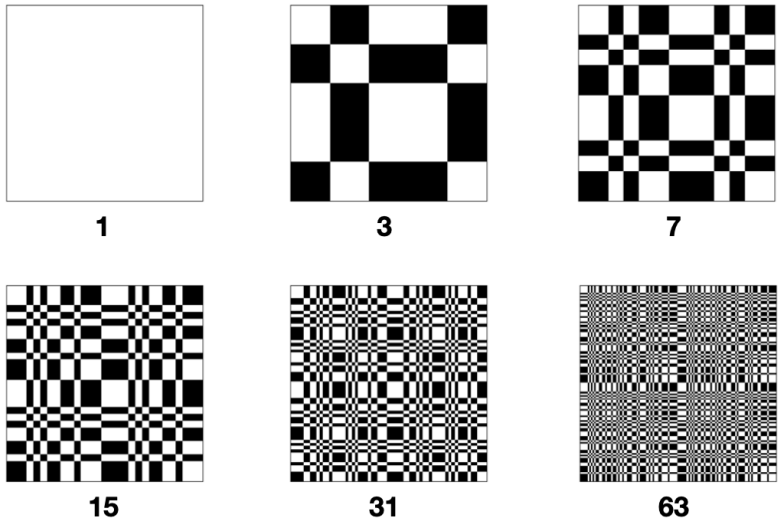

any convenience at all. The reason is this: the near-field effects map in exactly the opposite direction to the occlusion effects! Consider a setup with the scene plane at $y = 1$, the observation plane at $y = -1$, and the occluder frame at $y = 0$. Suppose that the occluder frame includes an aperture (meaning no occlusion) at the point $(x, y) = (0, 0)$. Now each point on the observation is guaranteed a contribution from the point across from it in the scene; that is, a point at $(x, -1)$ on the observation is guaranteed a contribution from point $(-x, 1)$ in the scene. It's that negation that drove us to swap the index order of scene and observation, so that scene went from $-x_{max}$ to x_{max}) and observation from x_{max} to $-x_{max}$.

But now let's think about the near-field effects. Ignoring the effects of occlusion, a point at $(x, -1)$ on the observation will get the most light from the point nearest to it in the scene—that is, $(x, 1)$. That light will fall off as $I = y/(x^2 + y^2)$, as we saw earlier. This is exactly the reverse of the occlusion phenomenon. So if the diagonals of constancy of transfer matrices in a world with occlusion but no near-field effects go from upper-left to lower-right, the diagonals of constancy of transfer matrices in a world *without* occlusion, but *with* near-field effects, must go from upper-right to lower-left. We just can't win!

So what happens when we have both occlusion and near-field effects? The answer is simple: we take the Hadamard product—i.e. the elementwise product—of the two transfer matrices with each individual effect. And this leads to the next unfortunate consequence of considering near-field effects in our analysis: the Hadamard product is a "disrespectful" operation. By this I mean that it doesn't treat the matrices as functions of vectors to other vectors; rather, it treats them only as boxes of numbers. When you introduce disrespectful operations into your setup, it becomes very difficult to say anything analytically about the result. And so, even though it's easy for us to say a lot about the transfer matrix from occlusion, and also easy for us to say a lot about the transfer matrix from near-field effects, it's not at all easy for us to say much about the combined transfer matrix: their Hadamard product. At least, it's not easy for us to say much analytically. We can still say interesting things about it through a combination of common sense and simulations.

Let's start with the common sense. When the scene is close enough to the observation plane, the near-field effects are effectively a blurry pinhole, but one that treats the scene as reversed relative to how an actual blurry pinhole would treat the scene. (See Figure **??**.) When we take the Hadamard product of these two matrices, it's intuitive that it would the determinant of the matrix that results. After all, the determinant of a matrix is a sum of permutations; when we take the Hadamard product of these two matrices whose permutations are non-overlapping, it makes sense that they would interact destructively. In other words, it won't help to have both the near-field effect and the occlusion effect happening at once; the result won't be better than either having the near-field effect alone, or the occlusion effect alone. Which one of those two is better, of course depends on the details: what occluder are we talking about, and how strong is the near-field effect?

If we're to talk about which occluder is *optimal* under these conditions, we might expect, then, that while near-field effects are week, the optimal occluder continues to be whatever was optimal without the near-field effects; as we gradually strengthen the near-field effects, at some point the optimal occluder will suddenly switch to being a completely open aperture. This should happen once a simple pinhole starts outperforming a spectrally-flat occluder that is being marred by increasingly strong near-field effects.

And indeed, that's what we see in our simulations! See Figure **??**.

2.7 The Optimal Pinhole

What size of pinhole is optimal, given our standard assumptions? This might seem to be an irrelevant question—the optimal occluding frame is not a pinhole, so why should we care what size of pinhole is optimal?

Well, it is a simple enough question that we are able to solve it analytically, which is nice. It can come up that you only have a pinhole and all you can control is its size. It is a good and intuitive test case for a lot of the mutual-information-based machinery that has been introduced so far. But more importantly, it will later be

useful for us to have analyzed this question, as the idea of a "wide pinhole" will be a useful analogy for near-field effects.

First of all, at a high level, what is the fundamental tradeoff around pinhole size? The answer is that smaller pinholes let in less light, but larger pinholes give you a blurrier image. If you're nearsighted, you can see this tradeoff in action by squinting—squinting lets you get sharper view of whatever it is you're looking at, but squint too much and you won't have enough light! It's intuitive, then, that a high SNR would make the optimal pinhole smaller (to get a sharper image), whereas a low SNR would make the optimal pinhole larger (to get more total light). Indeed, this is exactly what our pupils do! But it's satisfying to see this justified by our information-theoretic model.

2.8 Optimal phase arrays

The earlier bound on the determinants of

Chapter 3

Occluder-based Imaging with Real Occluders

3.1 Turning Corners into Cameras

3.1.1 Introduction

"Turning Corners into Cameras" is the pithy name for one of the simplest imaging occluder-based imaging techniques—but also one of the most robust, effective, and practical. Although the idea is now years old, I still use it as my first example whenever I want to explain how one might use occluders to image hidden scenes using visible light. And although there's still plenty of work to be done before it could be sold as a product (perhaps to be used in self-driving cars) it is in my own estimation the single likeliest thing in this thesis, or in the subfield of passive visible-light NLoS imaging (that I know of), to be put to practical use in the near future.

So what's the idea? The idea is to use the corner as an edge occluder. In the language of the previous chapter, the "occluding frame" is a half-occluding, half-transmitting frame. The transfer matrix that gives you is an upper-triangular matrix. Certainly this matrix will be far from optimal by the standards of the previous chapter! But it's simple and ubiquitous, and if all you're looking for is a 1D reconstruction of the hidden scene, it will work well enough.

This particular type of occluder also has the additional nice property of having, like the pinhole, a particularly recognizable reconstruction algorithm. A pinhole inverts (and blurs) the scene but otherwise doesn't distort it, so that the observation matches the image; an edge occluder integrates the scene, so that if the scene intensity function is $f(x)$, the observation intensity function will be $\int f(x)dx$. That means that in order to reconstruct, all you have to do is take the derivative of your scene with respect to space. This is convenient not only because it means the core algorithm is simple, but also because some cameras already exist which automatically record spatial derivatives at the hardware level [**?**].

The headline figure from *Turning Corners into Cameras* explains this idea well; see Fig. 3-1. Note how the colors on the floor give us a 1D view of what's in the scene, integrated over space. This is exactly what we expected to see from an edge occluder, given our analysis in the previous chapter. The fact that in this case, the observation plane (i.e. the floor) is perpendicular to the occluder frame (i.e. the wall) is what makes the spatial variation on the floor be a function of angle from the wall, rather than just the x-coordinate. (This phenomenon will be one I go into in more detail later.)

3.1.2 Edge cameras in practice

An edge camera system consists of four components: the visible and hidden scenes, the occluding edge, and the ground, which reflects light from both scenes. We refer to the (ground) plane perpendicular to the occluding edge as the *observation plane*. By analyzing subtle variations in the penumbra at the base of an edge, we are able to deduce a hidden subject's pattern of motion.

The reflected light from a surface at point p is a function of the incoming light L_i' as well as the surface's albedo a and BRDF β. Specifically,

$$L_o'(p, \hat{v}_o) = a(p) \int L_i'(p, \hat{v}_i)\, \beta(\hat{v}_i, \hat{v}_o, \hat{n})\, \gamma(\hat{v}_i, \hat{n})\, \mathrm{d}\hat{v}_i, \tag{3.1}$$

where $\hat{v}_i$ and $\hat{v}_o$ denote the incoming and outgoing unit vectors of light at position

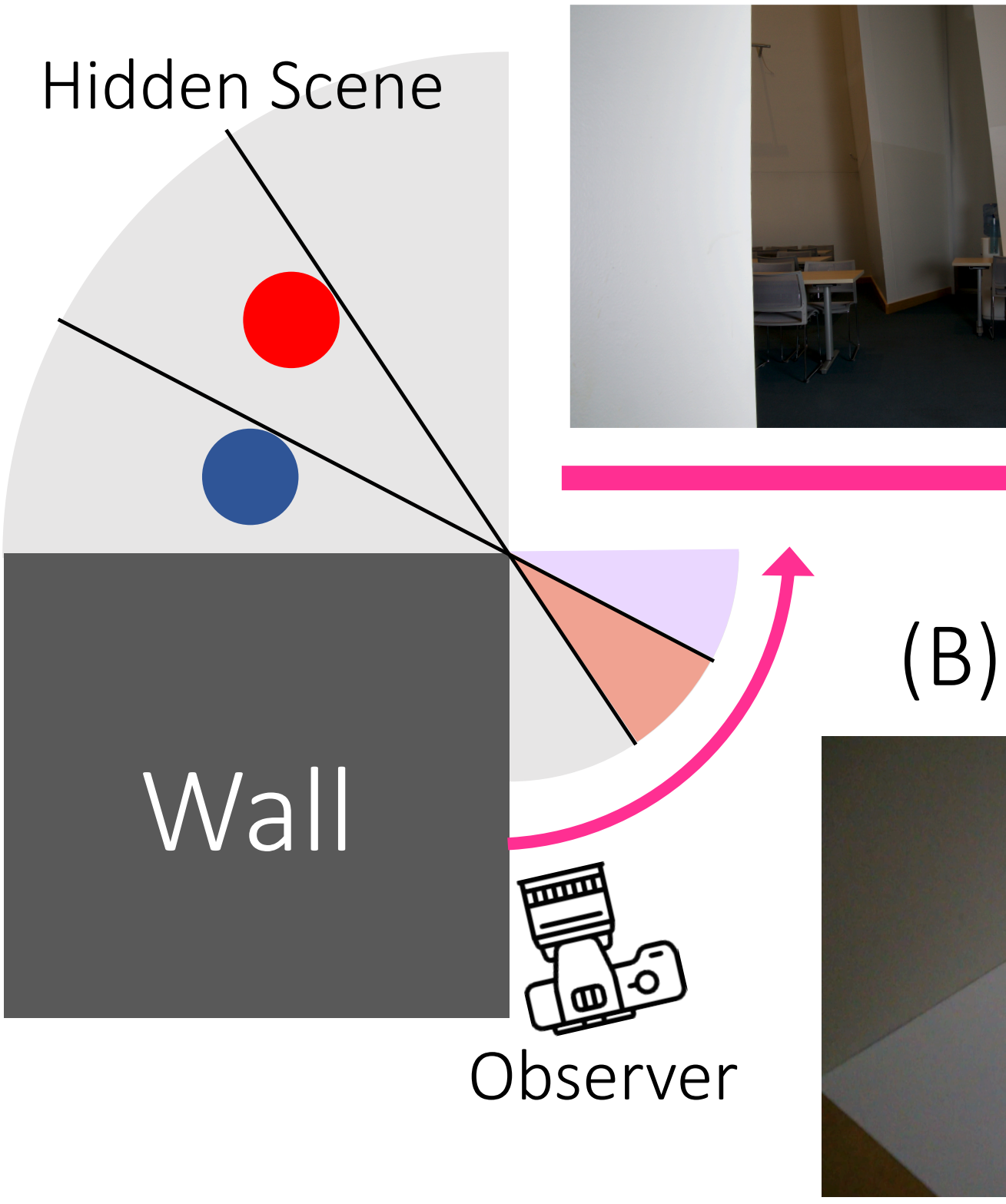

Figure 3-1: A method for constructing a 1-D video of an obscured scene. The far left shows a diagram of a typical scenario: two people—one wearing red and the other blue—are hidden from view by a wall. To an observer walking around the

$p = (r, \theta)$, respectively, and $\gamma(\hat{v}_i, \hat{n}) = \frac{\hat{v}_i \cdot \hat{n}}{\hat{v}_i \hat{n}}$. We parameterize p in polar coordinates, with the origin centered at the occluding edge and $\theta = 0$ corresponding to the angle parallel to the wall coming from the corner (refer to Fig. 3-2). For simplicity, we assume the observation plane is Lambertian, and that the visible and hidden scene are modeled as light emitted from a large celestial sphere, parameterized by right ascension α and declination δ. Under these assumptions, we simplify (3.1):

$$L'_o(r, \theta) = a(r, \theta) \int_{\alpha=0}^{2\pi} \int_{\delta=0}^{\pi/2} L_i(\alpha, \delta) \, \mathrm{d}\alpha \, \mathrm{d}\delta \tag{3.2}$$

where $L_i(\alpha, \delta) = L'_i(\alpha, \delta)\gamma(\alpha, \delta)$. Furthermore, since the occluding edge blocks light from $[\pi + \theta, 2\pi]$ at radial line θ,

$$L'_o(r, \theta) = a(r, \theta) \left[L_v + \int_{\phi=0}^{\theta} L_h(\phi) \, \mathrm{d}\phi \right] \tag{3.3}$$

for $L_v = \int_{\alpha=0}^{\pi} \int_{\delta=0}^{\pi/2} L_i(\alpha, \delta) \, \mathrm{d}\alpha \, \mathrm{d}\delta$ and $L_h(\phi) = \int_{\delta=0}^{\pi/2} L_i(\pi + \phi, \delta) \, \mathrm{d}\delta$. By inspecting (3.3) we can see that the intensity of light on the penumbra is explained by a constant term, L_v, which is the contribution due to light visible to the observer, and a varying angle dependent term which integrates the light in the hidden scene, L_h. For instance, a radial line at $\theta = 0$ only integrates the light from the scene visible to the observer, while the radial line $\theta = \pi/2$ reflects the integral of light over the entire visible and hidden scenes.

Then, the derivative of the observed penumbra recovers the 1-D angular projection of the hidden scene:

$$\frac{\mathrm{d}}{\mathrm{d}\theta} L'_o(r, \theta) = a(r, \theta) \, L_h(\phi). \tag{3.4}$$

But what happens if someone walks into the hidden scene at time t, changing $L_h^0(\phi)$ to $L_h^t(\phi)$? In this case, the spatial derivative of the temporal difference encodes the angular change in lighting:

$$\frac{d}{d\theta} \left[L'^t_o(r, \theta) - L'^0_o(r, \theta) \right] = a(r, \theta) \left[L_h^t(\theta) - L_h^0(\theta) \right] \tag{3.5}$$

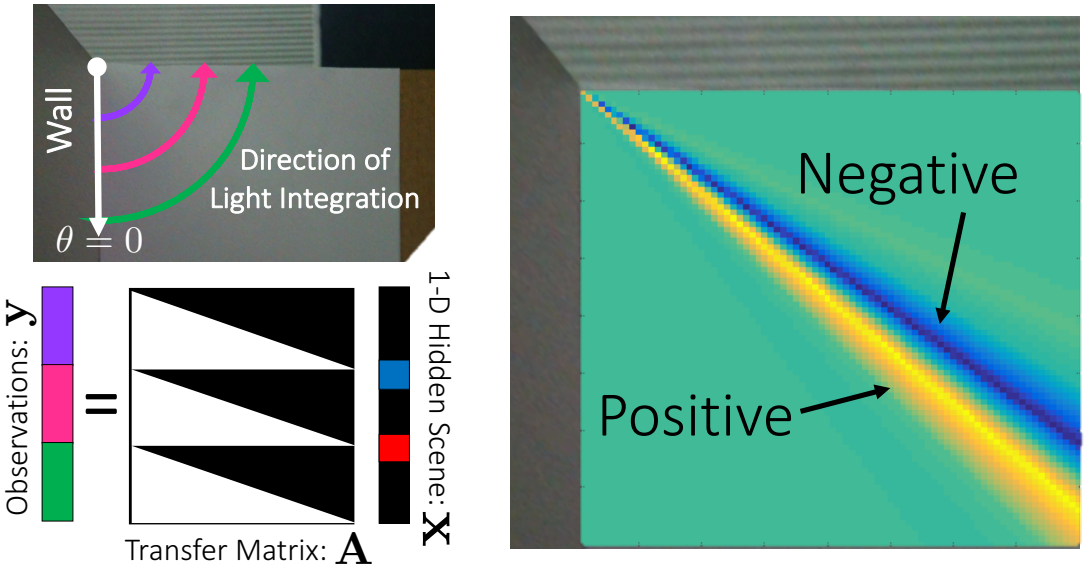

(A) Constructing Transfer Matrix (B) Sample Estimation Gain Image

Figure 3-2: In (A), the transfer matrix, $\mathbf{A}$, is shown for a toy situation in which observations lie along circles around the edge. In this case, $\mathbf{A}$ would simply be a repeated lower triangular matrix. (B) contains an example estimation gain image, which describes the matrix operation performed on observations $\mathbf{y}^{(t)}$ to estimate $\mathbf{x}^{(t)}$. As predicted, the image indicates that we are essentially performing an angular derivative in recovering a frame of the 1-D video.

In other words, the angular derivative of the penumbra's difference from the reference frame is a signal that indicates the angular change in the hidden scene over time. In practice, we obtain good results assuming $a(r, \theta) = 1$ and using the cameras' native encoded intensity values.

3.1.3 Method

Using a video recording of the observation plane, we generate a 1-D video indicating the changes in a hidden scene over time. These 1-D angular projections of the hidden scene viewed over many time-steps reveal the trajectory of a moving object behind the occluding edge.

Likelihood: At each time t, we relate the observed M-pixels on the projection plane, $\mathbf{y}^{(t)}$, to the 1-D angular projection of the hidden scene, $L_h^{(t)}(\phi)$. We formulate a discrete approximation to our edge camera system by describing the continuous

image $L_h^{(t)}(\phi)$ using N terms, $\mathbf{x}^{(t)}$. The observations $\mathbf{y}^{(t)}$ then relate to the unknown parameters $\mathbf{x}^{(t)}$ and $L_v^{(t)}$ by a linear matrix operation:

$$\mathbf{y}^{(t)} = L_v^{(t)} + \mathbf{A}\mathbf{x}^{(t)} + \mathbf{w}^{(t)}, \qquad \mathbf{w}^{(t)} \sim \mathcal{N}(0, \lambda^2 \mathbf{I}),$$

where the $M \times N$ matrix $\mathbf{A}$ is defined by the geometry of the system. More explicitly, each row m of $\mathbf{A}$ integrates the portion of the hidden scene visible from observation m, $\mathbf{y}_m^{(t)}$. In the simplified case of observations that lie on a circle around the occluding edge, $\mathbf{A}$ would simply be a constant lower-triangular matrix; see Fig. 3-2A.

Let $\widetilde{\mathbf{A}}$ be the column augmented matrix $[\mathbf{1}\ \mathbf{A}]$. We can then express the likelihood of an observation given $\mathbf{x}^{(t)}$ and $L_v^{(t)}$ as:

$$p(\mathbf{y}^{(t)}|\mathbf{x}^{(t)}, L_v^{(t)}) = \mathcal{N}\left(\widetilde{\mathbf{A}}\left[L_v^{(t)}\ \mathbf{x}^{(t)T}\right]^T, \lambda^2\mathbf{I}\right). \tag{3.6}$$

Prior: The signal we are trying to extract is very small relative to the total light intensity on the observation plane. Therefore, to improve the quality of results, we enforce spatial smoothness of $\mathbf{x}^{(t)}$. We use a simple L2 smoothness regularization over adjacent parameters in $\mathbf{x}^{(t)}$. This corresponds, for a gradient matrix $\mathbf{G}$, to using the prior

$$\begin{aligned} p(\mathbf{x}^{(t)}) &\propto \prod_{n=1}^{N-1} \exp\left[-\frac{1}{2\sigma^2}\|\mathbf{x}^{(t)}[n] - \mathbf{x}^{(t)}[n-1]\|_2^2\right] \\ &= \mathcal{N}(0, \sigma^2(\mathbf{G}^T\mathbf{G})^{-1}). \end{aligned} \tag{3.7}$$

Inference: We seek a maximum a posteriori (MAP) estimate of the hidden image coefficients, $\mathbf{x}^{(t)}$, given M observations, $\mathbf{y}^{(t)}$, measured by the camera. By combining the defined Gaussian likelihood and prior distributions, we obtain a Gaussian posterior distribution of $\mathbf{x}^{(t)}$ and $L_v^{(t)}$,

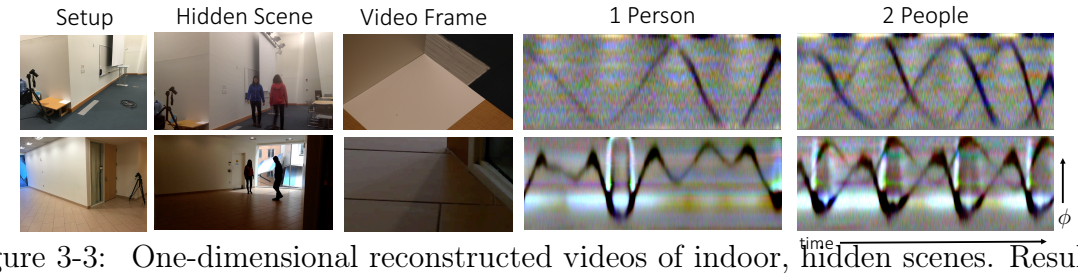

Figure 3-3: One-dimensional reconstructed videos of indoor, hidden scenes. Results are shown as space-time images for sequences where one or two people were walking behind the corner. In these reconstructions, the angular position of a person, as well as the number of people, can be clearly identified. Bright line artifacts are caused by additional shadows appearing on the penumbra.

$$
\begin{aligned}
p(\mathbf{x}^{(t)}, L_v^{(t)} | \mathbf{y}^{(t)}) &= \mathcal{N}\left(\left[\hat{L}_v^{(t)} \ \hat{\mathbf{x}}^{(t)T} \right]^T, \Sigma^{(t)} \right) \\
\Sigma^{(t)} &= \left[\lambda^{-2} \widetilde{\mathbf{A}}^T \widetilde{\mathbf{A}} + \sigma^{-2} \begin{pmatrix} \mathbf{0} & \mathbf{0} \\ \mathbf{0} & \mathbf{G}^T\mathbf{G} \end{pmatrix} \right]^{-1} \\
\left[\hat{L}_v^{(t)} \ \hat{\mathbf{x}}^{(t)T} \right]^T &= \Sigma^{(t)} \lambda^{-2} \widetilde{\mathbf{A}}^T \mathbf{y}^{(t)}
\end{aligned} \tag{3.8}
$$

where the maximum a posteriori estimate is given by $\hat{\mathbf{x}}^{(t)}$.

To better understand the operation that is being performed to obtain the 1-D reconstruction, we visualize each row of the matrix $\Sigma^{(t)} \lambda^{-2} \widetilde{\mathbf{A}}^T$. We refer to each reshaped row of this matrix as the *estimation gain image*. An example estimation gain image is shown in Fig. 3-2B. Note that, as expected, the matrix operation is computing an angular derivative over the observation plane.

Implementation Details

Rectification: All of our analysis thus far has assumed we are observing the floor parallel to the occluding edge. However, in most situations, the camera will be observing the projection plane at an angle. In order to make the construction of the matrix $\mathbf{A}$ easier, we begin by rectifying our images using a homography. In these results, we assume the ground is perpendicular to the occluding edge, and estimate the homography using either a calibration grid or regular patterns, such as tiles, that naturally appear on the ground. Alternatively, a known camera calibration could be

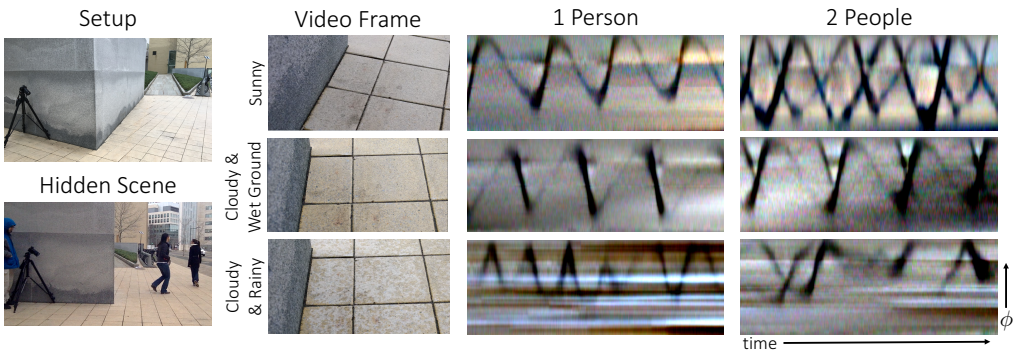

Figure 3-4: 1-D reconstructed videos of a common outdoor, hidden scene under various weather conditions. Results are shown as space-time images. The last row shows results from sequences taken while it was beginning to rain. Although artifacts appear due to the appearing raindrops, motion trajectories can be identified in all reconstructions.

used.

Background Subtraction: Since we are interested in identifying temporal differences in a hidden scene due to a moving subject, we must remove the effect of the scene's background illumination. Although this could be accomplished by first subtracting a background frame, L_o^0, taken without the subject, we avoid requiring the availability of such a frame. Instead, we assume the subject's motion is roughly uniform over the video, and use the video's mean image in lieu of a true background frame.

Temporal Smoothness: In addition to spatial smoothness we could also impose temporal smoothness on our MAP estimate. $\hat{\mathbf{x}}^{(t)}$. This helps to further regularize our result, at the cost of some temporal blurring. However, to emphasis the coherence among results, we do not impose this additional constraint. Each 1-D image, $\mathbf{x}^{(t)}$, that we show is independently computed. Results obtained with temporal smoothness constraints are shown in the supplemental material.

Parameter Selection: The noise parameter λ^2 is set for each video as the median variance of estimated sensor noise. The spatial smoothness parameter, σ, is set to 0.1 for all results.

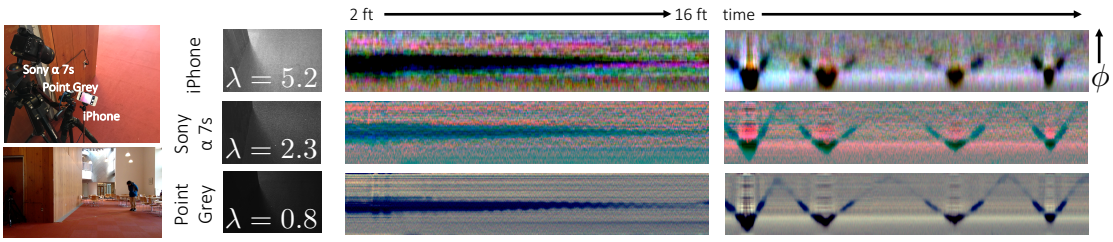

Figure 3-5: The result of using different cameras on the reconstruction of the same sequence in an indoor setting. Three different 8-bit cameras (an iPhone 5s, a Sony Alpha 7s SLR, and an uncompressed RGB Point Grey) simultaneously recorded the carpeted floor. Each camera introduced a different level of per-pixel sensor noise. The estimated standard deviation of sensor noise, λ, is shown in (B). We compare the quality of two sequences in (C) and (D). In (C), we have reconstructed a video from a sequence of a single person walking directly away from the corner from 2 to 16 feet at a 45 degree angle from the occluded wall. This experiment helps to illustrate how signal strength varies with distance from the corner. In (D), we have done a reconstruction of a single person walking in a random pattern.

3.1.4 Experiments and Results

Our algorithm reconstructs a 1-D video of a hidden scene from behind an occluding edge, allowing users to track the motions of obscured, moving objects. In all results shown, the subject was not visible to an observer at the camera.

We present results using space-time images. These images contain curves that indicate the angular trajectories of moving people. All results, unless specified otherwise, were generated from standard, compressed video taken with a SLR camera. Please refer to the supplemental video for full sequences and additional results.

Environments

We show several applications of our algorithm in various indoor and outdoor environments. For each environment, we show the reconstructions obtained when one or two people were moving in the hidden scene.

Indoor: In Fig. 3-1 we show a result obtained from a video recorded in a mostly dark room. A large diffuse light illuminated two hidden subjects wearing red and blue clothing. As the subjects walked around the room, their clothing reflected light, allowing us to reconstruct a 1-D video of colored trajectories. As correctly reflected

in our constructed video, the subject in blue occludes the subject in red three times before the subject in red becomes the occluder.

Fig. 3-3 shows additional examples of 1-D videos recovered from indoor edge cameras. In these sequences, the environment was well-lit. The subjects occluded the bright ambient light, resulting in the reconstruction's dark trajectory. Note that in all the reconstructions, it is possible to count the number of people in the hidden scene, and to recover important information such as their angular size and speed, and the characteristics of their motion.

Outdoor: In Fig. 3-4 we show the results of a number of videos taken at a common outdoor location, but in different weather conditions. The top sequences were recorded during a sunny day, while the bottom two sequences were recorded while it was cloudy. Additionally, in the bottom sequence, raindrops appeared on the ground *during* recording, while in the middle sequence the ground was fully saturated with water. Although the raindrops cause artifacts in the reconstructed space-time images, you can still discern the trajectory of people hidden behind the wall.

Video Quality:

In all experiments shown thus far we have used standard, compressed video captured using a SLR camera. However, video compression can create large, correlated noise that may affect our signal. We have explored the effect video quality has on results. To do this, we filmed a common scene using 3 different cameras: an iPhone 5s, a Sony Alpha 7s SLR, and a uncompressed RGB Point Grey. Fig. 3-5 shows the results of this experiment assuming different levels of i.i.d. noise. Each resulting 1-D image was reconstructed from a single frame. The cell phone camera's compressed videos resulted in the noisiest reconstructions, but even those results still capture key features of the subject's path.

Velocity Estimation

The derivative of a person's trajectory over time, $\phi^{(t)}$, indicates their angular velocity. Fig. **??** shows an example of the estimated angular velocity obtained from a single

edge camera when the hidden subject was walking roughly in a circle. Note that the person's angular size and speed are both larger when the person is closer to the corner. Such cues can help approximate the subject's 2-D position over time.

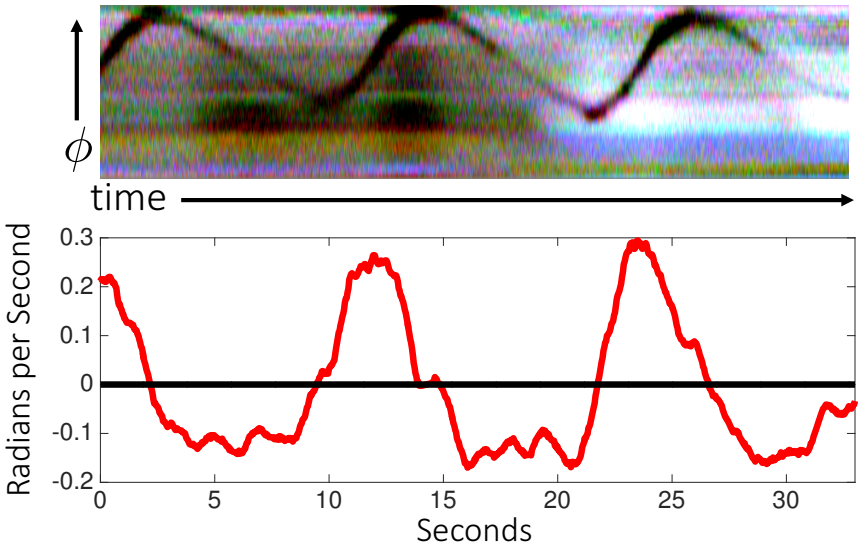

Figure 3-6: A subject's reconstructed angular velocity relative to the corner as a function of time. In this sequence, a person was walking in circles far from the corner.

Appendix A

Tables

Table 1: Armadillos

Armadillos	are
our	friends

Appendix B

Figures

Figure B-1: Armadillo slaying lawyer.

Figure B-2: Armadillo eradicating national debt.